MDC G0596

EVALUATION OF A LIGHT-GAS GUN HYPERVELOCITY AUGMENTATION TECHNIQUE FINAL REPORT

MAY 1970

Prepared under Contract No. NAS9-9312
by McDonnell Douglas Astronautics Company—Western Division
Huntington Beach, California
for
NATIONAL AERONAUTICS AND SPACE ADMINISTRATION

NASA CR 108494

MDC G0596

EVALUATION OF A LIGHT-GAS GUN HYPERVELOCITY AUGMENTATION TECHNIQUE FINAL REPORT

MAY 1970

by
R. N. TENG

Prepared under Contract No. NAS9-9312
by McDonnell Douglas Astronautics Company–Western Division
Huntington Beach, California
for
NATIONAL AERONAUTICS AND SPACE ADMINISTRATION

PRECEDING PAGE BLANK NOT FILMED.

PREFACE

This report was prepared by the McDonnell Douglas Astronautics Company--Western Division, under NASA Contract NAS 9-9312. The investigation was initiated by the Manned Spacecraft Center of NASA, Houston, to evaluate a light-gas gun hypervelocity augmentation technique. This work was administered under the direction of the Meteoroid Science Branch, B. C. Cour-Palais, Project Manager.

The report covers the complete work period from 24 March 1969 through 23 May 1970. It is submitted in partial fulfillment of Contract NAS 9-9312 and is cataloged by McDonnell Douglas as MDC G0596.

At McDonnell Douglas, Dr. J. L. Waisman, Director of Research and Development, and Dr. H. H. Dixon, Chief Engineer of the Advance Structures and Mechanical Department provided technical direction; G. L. Roark acted as program manager, and R. N. Teng was study director.

At the Douglas Aerophysics Laboratory, M. Hahner directed the light-gas gun operation and R. C. Curtis supervised the instrumentation.

The analysis of the constant base-pressure launch-cycle was the contribution of Dr. R. S. Hickman.

PRECEDING PAGE BLANK NOT FILMED.

ABSTRACT

An analysis of the interior ballistics of a constant base-pressure (CBP) gun is made, relating the muzzle velocity to pertinent initial conditions in the gun. The specific chamber volume history required for the CBP launch cycle and the method of approximating the chamber volume are presented. Fifty-two runs have been made with the light-gas gun at the Douglas Aerophysic Laboratory to verify the theory and to identify the important parameters which may affect its performance. The departure of the CBP theory from the experimental results has been identified as the friction between the piston and the high pressure section walls. Four types of collapsible pistons have been developed to meet the requirements of the CBP launch cycle. The collapsible-piston designs have been demonstrated to be particularly effective in damping out sharp pressure peaks during maximum performance runs.

CONTENTS

NOMENCLATURE

a	Non-dimensional sound speed, C/C_s
A	Area
C	Sound speed
G	Constant of integration
L	Length of piston collapse
M	Mach number or measure of sabot
P	Pressure
R	Gas constant
S	Entropy
T	Non-dimensional time $P_s A_s t/M_s C_s$, or temperature
t	Dimensional time
U	Dimensional velocity
V	Non-dimensional velocity U/C_s, or chamber volume
$\overline{V}$	Chamber volume
v	Specific volume
W	Mass of gas
w	Mass, rate of flow
X	Non-dimensional distance $= \dfrac{P_s A_s}{M_s C_s^2} x$
x	Dimensional distance
Z	$\dfrac{T^2}{2}$ -X, or $\sqrt{\dfrac{\gamma-1}{2}}$ V always a dummy variable
ϕ	$\sin^{-1} Z$
ρ	Mass density
θ	T/T_s, temperature ratio
π	P/P_s
γ	Specific heat ratio

Subscripts

i	Initial loading conditions
o	Original chamber conditions
s	Initial sabot conditions
r	Recession of collapsing piston
e	Barrel entrance
P	P characteristic, or piston velocity
c	Chamber
L	Local position of gas which first became sonic
q	Q characteristic
r	Required for constant base pressure operations
g	Gas
u	Required times for constant base pressure

Superscripts

*	Sonic conditions
1	Intermediate stations

Section 1
INTRODUCTION

Laboratory simulation of high velocity meteoroid impact against spacecraft plays an important role in the design of space hardware. The combination of a light-gas gun and a ballistic range provides an excellent facility for impact data acquisition. Unfortunately, the maximum projectile velocity obtainable from such a facility falls far short of that of a real meteoroid in space. For this reason, considerable attention has been paid to the development of the light-gas gun to achieve higher velocity.

A light-gas gun usually consists of a pump tube containing a piston, a taper section, and a launch tube holding a model cradled in a sabot (Figure 1-1). Gun powder is used to accelerate the piston which in turn compresses and heats the pump-tube gas (usually hydrogen). When the desired pressure is achieved in the taper section, a diaphragm at the launch-tube entrance breaks and the sabot is sent down the launch tube. After the sabot leaves the muzzle it is separated from the model by various stripping techniques and the model continues into the impact area.

To obtain maximum velocity the model should be subjected either to the maximum pressure (or acceleration) tolerable for structural integrity of the sabot and model, or the taper-section pressure should be held at its maximum allowable value. In the case in which the model base pressure must be limited, it is clear that for a given barrel length a maximum velocity will be obtained when the base pressure is held constant at its maximum value. The gun cycle which accomplishes this has been given the name constant base pressure cycle (CBP). (References 1, 2, and 3.)

If the breech pressure is limiting instead of the base pressure it is equally clear that maximum velocity will be achieved by holding breech pressure constant. This will result in an unsteady model-base pressure and a variable acceleration.

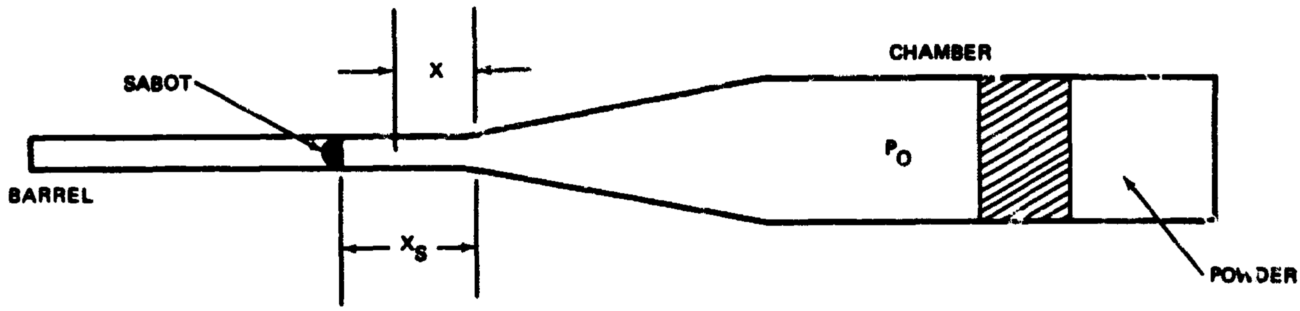

Figure 1-1. Hypervelocity Light-Gas Gun

Probably the most important and practical cycle is that in which the model pressure and the breech pressure must be held within specified limits so that during the early portion of the cycle the base pressure is held constant and later the breech pressure is constant.

This report describes a method of approximating the constant base pressure launch cycle by various piston designs.

For the purpose of simplifying discussion, the pump tube and the taper section will be designated as chamber. The launch tube will be represented by the barrel.

Section 2
THEORY OF CONSTANT BASE-PRESSURE GUN

2.1 SIMILARITY SOLUTION

2.1.1 Similarity Barrel Flow

The first launch cycle to be presented (References 1 and 2) is one in which the gas in the barrel moves exactly in step with the piston, and gaseous elements do not undergo any change in pressure or temperature. This cycle is called the similarity solution (Reference 3). Since the velocity is assumed to be only a function of time and since the base pressure is required to be constant, for the sabot or for any gas particle

$$V = T \tag{2-1}$$

where

$$V = U/C_s \text{ and}$$
$$T = P_s A_s t / M_s C_s$$

The sabot position in the barrel is

$$X = T_2/2 = \frac{P_s A_s}{M_s C_s^2} x \tag{2-2}$$

Now, in order that no compression or expansion waves change the base pressure (in fact, compression waves do reach the sabot, but are continuously cancelled by the expansion fan emanating from it), the entire column of gas in the barrel must experience the same velocity given by Equation (2-1) and must experience an acceleration $P_s A_s / M_s$. Using this fact, the pressure distribution in the barrel can be obtained by using either Curtis' argument

(Reference 1) (an analogy with an isentropic atmosphere subjected to an acceleration of gravity - P_sA_s/M_s), or with the aid of the equation

$$-\frac{1}{\rho}\frac{\partial P}{\partial x} = \frac{du}{dt} = \frac{P_sA_s}{M_s} \qquad (2-3)$$

and the isentropic condition $P \sim \rho^{\gamma}$ so that

$$-\left(\frac{P_s}{P}\right)^{\frac{1}{\gamma}} dP = \frac{P_sA_s\rho_s}{M_s}\, dx \qquad (2-4)$$

which yields for any position x.

$$\left(\frac{P}{P_s}\right)^{\gamma} = \pi = [1 + (\gamma - 1)(X_s - X]^{\frac{\gamma}{\gamma-1}} \qquad (2-5)$$

where

$$\pi = P/P_s$$

This equation will hold as long as the gas is isentropic. The temperature of the gas in the barrel is

$$\theta = \frac{T}{T_s} = \frac{C^2}{C_s^{\,2}} = \left(\frac{P}{P_s}\right)^{\frac{\gamma-1}{\gamma}} = 1 + (\gamma - 1)(X_s - X) \qquad (2-6)$$

where the sound speed variation is also indicated.

2.1.2 Barrel Entrance Conditions

At the barrel entrance, $x = 0$ so that Equations (2-5) and 2-6) become

$$\pi_e = \left[1 + (\gamma - 1)\, X_s\right]^{\gamma/\gamma-1} \qquad (2-7)$$

and

$$\theta_e = \frac{C_e^{\ 2}}{C_s^{\ 2}} = 1 + (\gamma - 1)\, X_s \tag{2-8}$$

The velocity here (and everywhere in the barrel) is still given by Equation (2-1).

We can calculate the Mach number at the barrel entrance using Equations (2-1) and (2-8) to yield

$$M_e = \frac{U_e}{\sqrt{\gamma R T_e}} = \frac{T}{\left[1 + (\gamma - 1)\frac{T^2}{2}\right]^{\frac{1}{2}}} \tag{2-9}$$

2.1.3 Sonic Conditions at Barrel Entrance

The time when the flow is first sonic at the entrance is given by Equation (2-9) with $M_e = 1$, hence

$$T^* = \left(\frac{2}{3 - \gamma}\right)^{\frac{1}{2}} \tag{2-10}$$

The velocity at which the flow is sonic at the entrance is just

$$V^* = T^* = \left(\frac{2}{3 - \gamma}\right)^{\frac{1}{2}} \tag{2-11}$$

and the location of the sabot when sonic flow is achieved is

$$X_s^* = \frac{1}{3 - \gamma} \tag{2-12}$$

Finally, the pressure at the barrel entrance is, using Equation (2-7) and (2-12)

$$\pi_e^* = \left(\frac{2}{3 - \gamma}\right)^{\frac{\gamma}{\gamma - 1}} \tag{2-13}$$

Observe that for large time, Equation (2-9) yields for $\gamma = 7/5$

$$\lim_{T \to \infty} M_e = \sqrt{\frac{2}{\gamma - 1}} = 2.24 \tag{2-14}$$

So that for isentropic flow, the flow at the barrel entrance must eventually be supersonic. In the case of a fixed- geometry chambered gun this is impossible with an area decrease since when $M_e = 1$ the flow will choke.

2.1.4 Barrel Conditions After Sonic Flow

For similarity flow, after the flow at the barrel entrance becomes sonic, the flow will choke and sonic conditions will be maintained thereafter. Now the question is how the gas in the chamber must be processed to maintain the required steady acceleration in the barrel and at the same time produce sonic flow at the entrance.

The flow between the chamber and the barrel entrance will still be isentropic so that, once the barrel conditions are found, the chamber conditions will follow.

For the similarity solution it still is required that the velocity everywhere be given by Equation (2-1); however, now the barrel entrance temperature must be

$$\theta_e = \frac{T_e}{T_s} = V^2 \tag{2-15}$$

In order that the flow at the entrance be sonic.

Using Equation (2-1) we have

$$\theta_e = T^2 \tag{2-16}$$

Consider a small element of gas which entered the barrel at an arbitrary time, T', where $T' > T^*$ (Figure 2-1). The distance, X', traveled into the barrel by that element of gas is just

$$X' = \int_{T'}^{T} V dt = \frac{T^2 - T'^2}{2} \tag{2-17}$$

The temperature of the element of gas at X' is given by Equation (2-16) with $T = T'$. The temperature of the gas must not change since the flow is assumed similar and $V = V(T)$ only. If the pressure (hence temperature) of a gas element were to change because of a compression or expansion wave, the local acceleration would change and $V = V(T, x)$. Therefore, we can find the temperature in the gas at the point X'. This is done by observing that the gas element at X' entered the barrel at T' and the required value of θ is from Equation (2-16).

$$\theta'(X') = T'^2 \tag{2-18}$$

Using Equation (2-17) for T'^2, Equation (2-18) becomes

$$\theta'(X') = T^2 - 2X' \tag{2-19}$$

or

$$\theta(X) = 2(X_s - X') \tag{2-20}$$

The pressure gradient along the tube still must produce the required acceleration so that Equation (2-3) still holds, and using the ideal gas law, $P = \rho RT$, Equation (2-3) and the ideal gas law can be combined to yield

$$\frac{dP}{dX} = -\frac{P_s A_s}{M_s} \frac{P}{RT}$$

and then using Equation (2-20) and using nondimensional variables

$$-\frac{d\pi}{\pi} = \frac{\gamma dx}{2(X_s - X)} \tag{2-21}$$

and we can finally write

$$\int_{\pi}^{\pi^*} \frac{d\pi}{\pi} = -\frac{\gamma}{2} \int_0^{X_L^*} \frac{dX}{(X_s - X)} \tag{2-22}$$

where the limits express the fact that only the gas entering the barrel after $T = T^*$ obeys Equation (2-20). The notation X_L^* indicates that one must integrate only to the local position of the gas which first became sonic. Note that if X_s were left in the terms of T that Equation (2-22) is independent of T and the same results would hold. The pressure gradient between fluid elements is independent of T or X_s. Equation (2-22) is easily integrated to yield

$$\frac{\pi_e}{\pi^*} = \left[\frac{X_s}{X_s - X_e}\right]^{\frac{\gamma}{2}} \tag{2-23}$$

We know from Equation (2-2) that $X_s = T^2/2$ and from Equation (2-15)

$$\pi^* = \left(\frac{2}{3 - \gamma}\right)^{\gamma/\gamma - 1}$$

Of course, the position of the gas exhibiting this pressure will move down the barrel.

Finally, we need X_L^*.

$$X_L^* = \int_{T^*}^{T} V dT = \frac{1}{2}\left(T^2 - T^{*2}\right) \tag{2-24}$$

Then

$$\frac{X_s}{X_s - X_L^*} = \frac{T^2}{T^{*2}} \tag{2-25}$$

$$\frac{X_s}{X_s - X_L} = \frac{T^2\,(3-\gamma)}{2} \tag{2-26}$$

Finally, the pressure at the barrel entrance is obtained by combining Equations (2-26), (2-2), (2-15) and (2-23).

$$\pi_e = \left(\frac{2}{3-\gamma}\right)^{\gamma/\gamma-1}\left(\frac{T}{T^*}\right)^{\gamma} \tag{2-27}$$

and since V = T

$$\pi_e = \left(\frac{2}{3-\gamma}\right)^{\frac{\gamma}{\gamma-1}}\left(\frac{V}{V^*}\right)^{\gamma} \tag{2-28}$$

Combining Equations (2-15) and (2-11) we get

$$\theta_e = \left(\frac{V}{V^*}\right)^2 \frac{2}{3-\gamma} \tag{2-29}$$

The entropy of a perfect gas may be written as

$$\frac{S_e - S_s}{\bar{R}} = \frac{\gamma}{\gamma-1}\ln\theta - \ln\pi \tag{2-30}$$

hence, using Equations (2-28) and (2-29)

$$\frac{S_e - S_s}{\bar{R}} = \frac{\gamma}{\gamma-1}\ln\left[\left(\frac{V}{V^*}\right)^2\frac{2}{3-\gamma}\right] - \ln\left(\frac{2}{3-\gamma}\right)^{\frac{\gamma}{\gamma-1}}\left(\frac{V}{V^*}\right)^{\gamma} \tag{2-31}$$

or

$$\frac{S_e - S}{R} = \gamma \frac{3 - \gamma}{\gamma - 1} \ln \frac{V}{V*} \tag{2-32}$$

Now $V > V*$ and $\gamma \left(\frac{3 - \gamma}{\gamma - 1}\right) > 0$, hence, the specific entropy at the barrel entrance and, hence, in the chamber, must increase in time after $V = V*$ for the similarity cycle. Thus, for a chambered gun it is impossible to construct a constant base-pressure similarity cycle unless the entropy in the chamber grows in time after sonic flow is first achieved at the barrel entrance.

If, instead of maintaining a constant entrance barrel area, the area of the barrel at its entrance is decreased by some mechanical means, it is conceivable that the isentropic condition could be maintained, especially in light of the fact that the isentropic barrel entrance Mach number exhibits a limit of 2.24. (Even though the Mach number exhibits a limit, both the velocity and the chamber temperature increase without limit). The required entropy behavior was first pointed out in Reference 3.

2.2 SIMILARITY-UNSTEADY SOLUTION

2.2.1 Barrel Conditions for Isentropic Constant Base-Pressure Flow

As was shown in Section 2.1.4, the specific entropy of the gas entering the barrel after sonic flow is achieved must increase if a similarity solution is to be followed. If the entropy is specified to be constant the similarity solution must be abandoned and the properties of fluid elements must be allowed to change after entry into the barrel. Figure 2-1 is an X, t, plot for a constant base cycle. The sabot curve is, of course, a parabola. As the sabot moves to the right in the barrel it creates expansion waves which travel to the left. At the sabot's rear face, compression waves must be arriving in just the proper fashion to reflect in a way that will maintain constant base-pressure. In fact, in the similarity solution, any element of gas has passing through it infinite trains of right running and left running waves which accelerate it unsteadily without changing the fluid elements, temperature, or pressure.

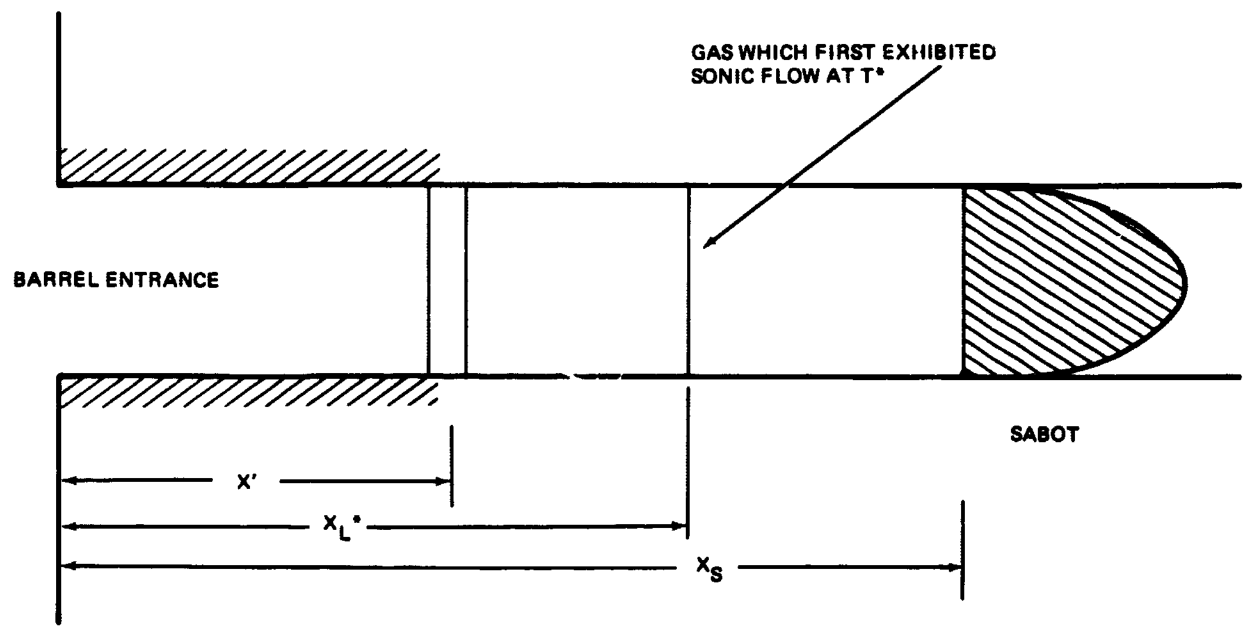

Figure 2-1. Relationship between Sabot and Gaseous Elements After Choking Occurs

It is possible to achieve constant base-pressure at the sabot if the flow field is governed by the similarity solution until sonic flow is achieved, and if the sonic entrance condition is coupled to a critical characteristic by an unsteady expansion in which fluid elements do not experience constant acceleration or pressure. We will choose to maintain the flow between the sabot and the Q characteristic which passes through the sonic point on the X-T diagram and which bounds an unsteady expansion thereafter.

For a Q characteristic we nave

$$\left.\frac{dX}{dT}\right|_q = V - a \qquad (2\text{-}33)$$

and along the limiting characteristic we know that

$$V = T \qquad (2\text{-}34)$$

since the flow to the right is in the similarity zone, and the nondimensional sound speed is

$$a = \left[1 + (\gamma - 1)\left(\frac{T^2}{2} - X\right)\right]^{\frac{1}{2}} \qquad (2\text{-}35)$$

hence,

$$\left.\frac{dX}{dT}\right|_q = T - \left[1 + (\gamma - 1)\left(\frac{T^2}{2} - X\right)\right]^{\frac{1}{2}} \qquad (2\text{-}36)$$

Now, if

$$Z = \frac{T^2}{2} - X$$

$$\frac{dZ}{dT} = T - \frac{dX}{dT}$$

$$\frac{dZ}{dT} = \left(1 + (\gamma - 1) Z\right)^{1/2} \qquad (2\text{-}37)$$

which integrates readily to

$$\frac{2}{\gamma - 1}\left[1 + (\gamma - 1)\left(\frac{T^2}{2} - X_q\right)\right]^{1/2} = T + G \qquad (2\text{-}38)$$

where G is a constant of integration.

For the Q characteristic passing through $X = 0$ when sonic flow begins, we have $T = \left(\frac{2}{3 - \gamma}\right)^{1/2}$ and Equation 2-38) can be arranged to yield the equation for the critical characteristic

$$X_q = \frac{1}{\gamma - 1}\left[1 - \left(\frac{\gamma - 1}{2} T + \sqrt{\frac{3 - \gamma}{2}}\right)^2\right] + \frac{T^2}{2} \qquad (2\text{-}39)$$

This characteristic is plotted in Figure 2-2.

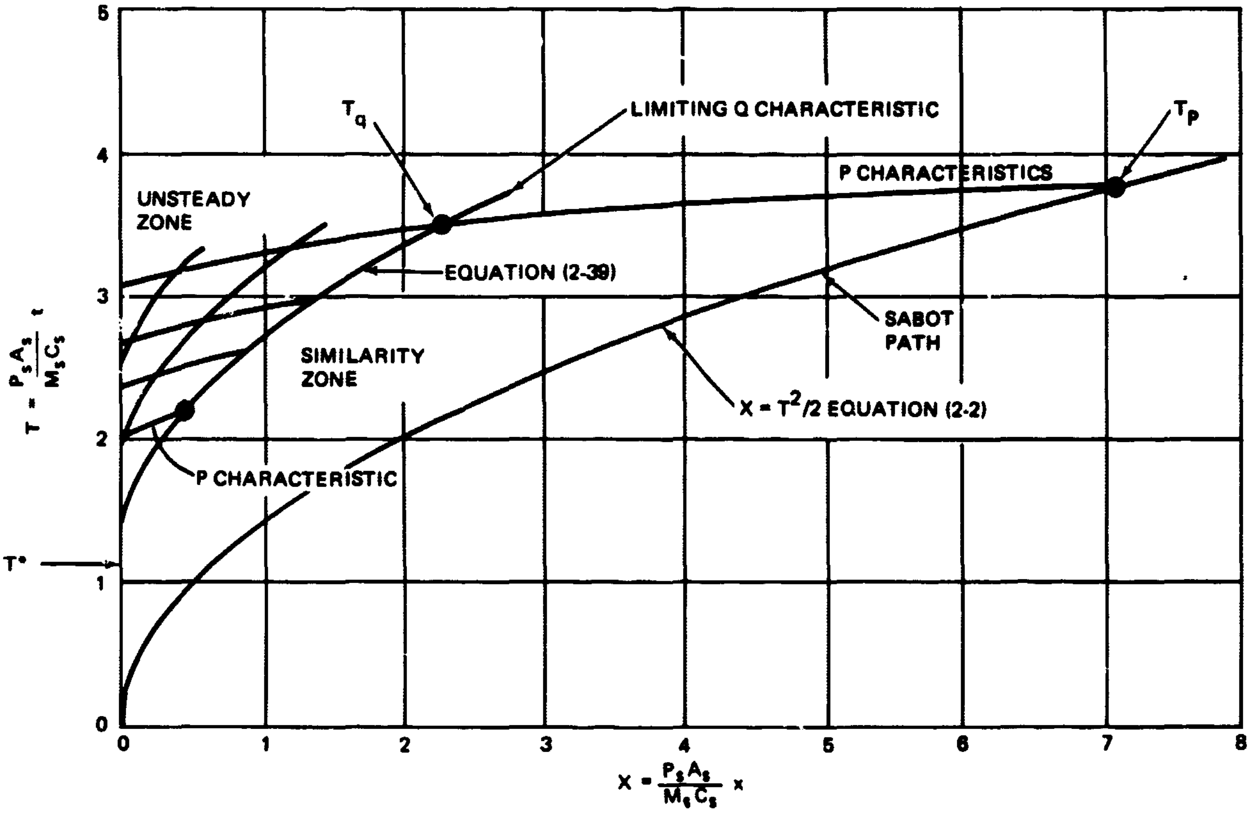

Figure 2-2. X-T Diagram of Sabot Launched with Similarity-Unsteady Cycle

The flow in the region between this limiting characteristic and the origin must be obtained using unsteady characteristics. The characteristic solution need be solved only once since X and T are nondimensionalized to include $P_s A_s / M_s$. The characteristic field in the unsteady zone of Figure 2-1 has been computed on an IBM 1620. The desired result is the barrel entrance velocity (or sound speed, since the flow is choked) as a function of time. This, coupled to the similarity solution for the subsonic flow, provides a time history of entrance velocity which will provide constant sabot base-pressure.

The details of the unsteady flow computations are quite straightforward. Suitable increments in time are chosen, and the Riemann invariants for left waves (P wave) are computed along the critical Q characteristic separating the similarity and unsteady zones. The first point on the sonic entrance is computed by averaging the physical slope of the first P wave from the first point on the Q characteristic computed at the Q wave, and at the origin. Since the common value of P is known, and since at the entrance V = a, the slope of a P wave at that point is easily computed. Once the first sonic point is known, a Q wave is generated in the unsteady region. The first point on this Q wave to the right of the origin will give the values at X = 0 for the next time calculated as above. This procedure is followed until a sufficient history of the flow at X = 0 is known.

Figure 2-3 is a plot of the entrance conditions as a function of time. For T < T* the flow is governed by similarity equations. After T > T* the unsteady-characteristics solution holds. As can be seen in Figure 2-3, the unsteady effect requires slightly higher sound speed, and considerably lower velocity at the inlet. The gas entering after T* accelerates unsteadily in the barrel.

2.2.2 Barrel Entrance Conditions for the Coupled Similarity - Unsteady Cycle

For T < T* the barrel entrance velocity is given by Equation (2-1) and the entrance sound speed by Equation (2-8). For T > T* the entrance velocity is given from the numerical solution shown in Figure 2-2.

The required entrance conditions are shown in Figure 2-3.

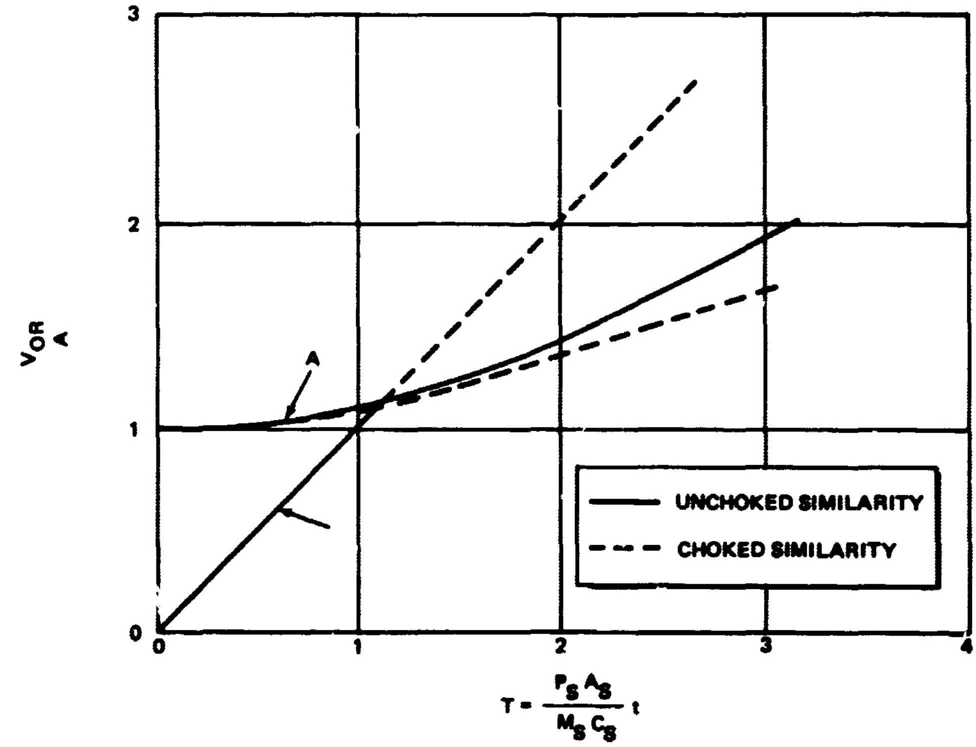

Figure 2-3. Required Barrel Entrance Conditions for Fixed-Geometry Chambered-Gun Constant Base-Pressure Launch Cycles

2.2.3 Mass Flow Into the Barrel ($T < T_{sonic}$)

The mass flow rate into the barrel is

$$w = \rho_e U_e A_s \tag{2-40}$$

and the total mass flow into the barrel is

$$W = \int_o^t w dt$$

which, using Equations (2-1) and (2-5) with $X = 0$, becomes

$$\frac{W}{M_s} = \int_o^T \gamma \left[1 + \frac{\gamma - 1}{2} T^2\right]^{\frac{1}{\gamma - 1}} T \, dT \tag{2-41}$$

or

$$\frac{W}{M_s} = \left[1 + \frac{\gamma - 1}{2} T^2\right]^{\frac{\gamma}{\gamma - 1}} - 1 \tag{2-42}$$

Note that this can be written using Equation (2-7) as

$$\frac{W}{M_s} = P_e/P_s - 1$$

2.2.4 Mass Flow Into the Barrel for Similarity - Unsteady Cycle ($T > T_{sonic}$)

Equation (2-40) still holds for mass flow into the barrel after $T = T^*$. However, the quadrature

$$W = \int_o^t w \, dt \tag{2-43}$$

cannot be solved in closed form since $U_e = U_e(t)$ is not in closed form. We can relate ρ_e/ρ_s to V since, in this cycle, the flow is still isentropic and ρ_e/ρ_s is equal to $a_e^{\frac{2}{\gamma-1}}$.

Then, using the fact that $V_e = a_e$

$$\frac{W}{M_s} = \frac{W*}{M_s} + \gamma \int_{T*}^{T} V_e^{\frac{\gamma+1}{\gamma-1}} \, dT \tag{2-44}$$

where V_e is obtained from Figure 2-3. Figure 2-4 is a plot of the mass required for the similarity-unsteady composite cycle assuming that all the gas is in the barrel at T. For $\gamma = 7/5$, $\frac{\gamma+1}{\gamma-1}$ is 6, so that $\frac{W}{M_s}$ grows rapidly with V_e.

It is of interest to note that even though the entrance velocity after sonic conditions is lower for the composite cycle, the density is higher, and the required mass for a given time of constant base pressure will be higher than for the similarity cycle.

The time of disturbance arrival at the sabot can be calculated by considering the path of a P wave in the similarity region. In this region

$$\begin{aligned} \frac{dX_p}{dT} &= a + V \\ &= T + \left[1 + (\gamma - 1)\left(\frac{T^2}{2} - X\right)\right]^{\frac{1}{2}} \end{aligned} \tag{2-45}$$

or, again letting $Z = T^2/2 - x$ and performing the required integrations for a P wave,

$$T_P + \frac{2}{\gamma - 1}\left[1 + (\gamma - 1)\left(\frac{T^2}{2} - X\right)\right]^{\frac{1}{2}} = G_p \tag{2-46}$$

where G_p is a constant for any P wave and Equation (2-46) describes the trajectory on the X-T plane of a P wave.

We can find G_p from the equation for the Q wave bounding the similarity region from the unsteady region. Using Equation (2-39)

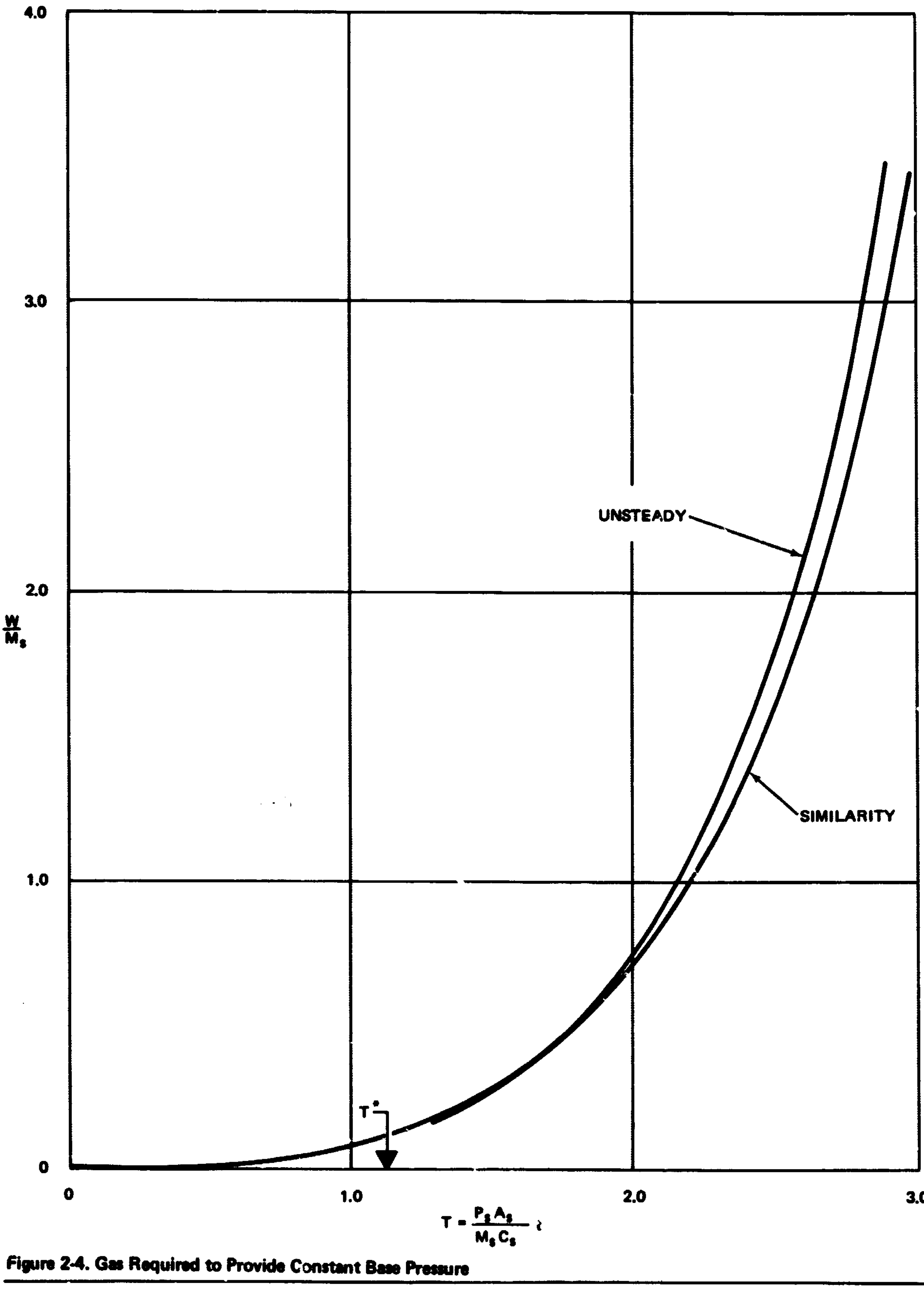

Figure 2-4. Gas Required to Provide Constant Base Pressure

$$\left[1 + (\gamma - 1)\left(\frac{T_q^2}{2} - X_q\right)\right]^{\frac{1}{2}} = \frac{\gamma - 1}{2} T_q + \sqrt{\frac{3 - \gamma}{2}} \qquad (2\text{-}47)$$

and upon substitution into Equation (2-45) and using the observation that at the sabot $\frac{1}{2} T_{su}^2 = X_p$, we have

$$T_p = 2 T_q + \frac{2}{\gamma - 1}\left[\sqrt{\frac{3 - \gamma}{2}} - 1\right] \qquad (2\text{-}48)$$

This equation allows one to relate the time of constant pressure behavior T_p, to the time that matched inlet conditions are required. In other words, to maintain constant base for T_p time, Equation (2-48) provides the value of T_q which then can be found from the numerical solutions. The time required to maintain the entrance conditions to achieve a time T_p of constant base-pressure is shown in Figure 2-5.

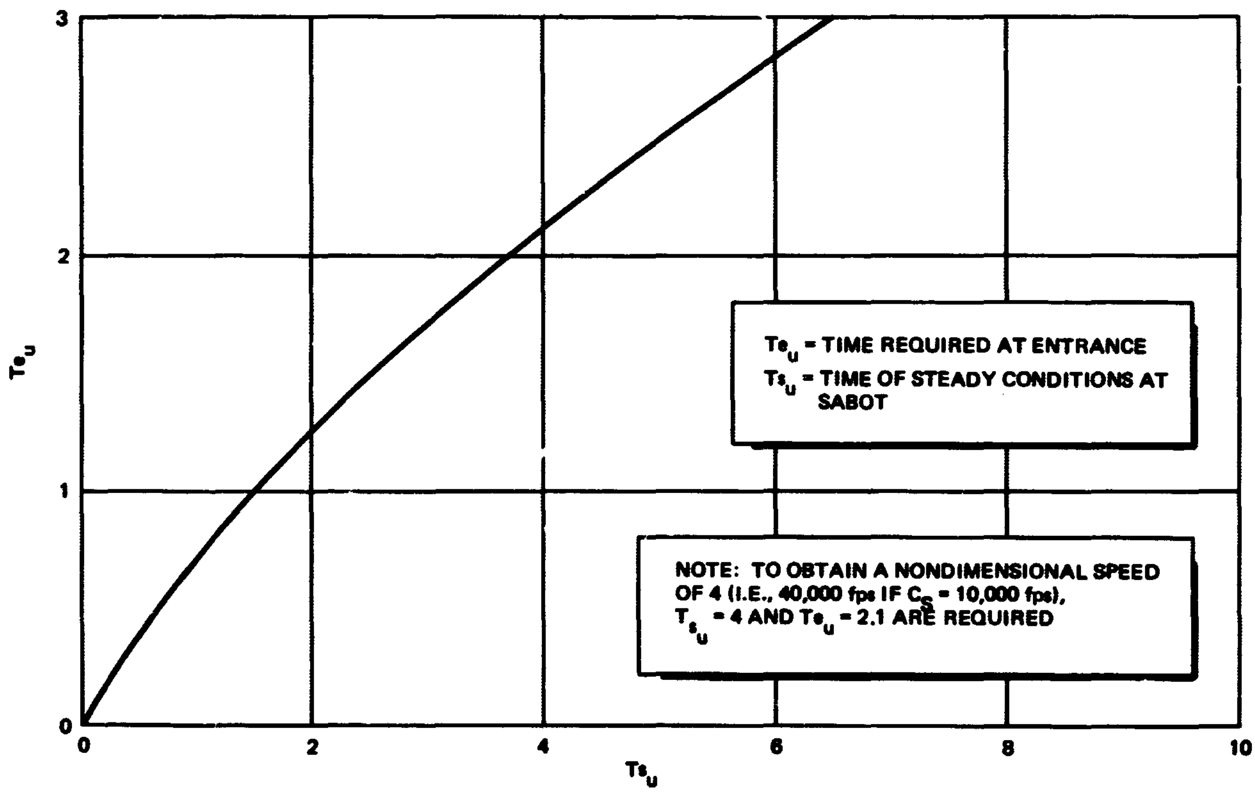

Figure 2-5. Constant Base Pressure Duration Vs Duration of Required Entrance Conditions

2.2.5 Chamber Conditions

2.2.5.1 Chamber Temperature and Pressure ($T < T^*$)

It is assumed that the flow between the chamber and the barrel is isentropic and quasi steady with $A_c >> A_s$. Then the steady energy equation yields

$$C_p T_c = C_p T_e + \frac{1}{2} U_e^2 \qquad (2\text{-}49)$$

Note that this equation covers both the similarity and similarity - unsteady cycles.

Now divide Equation (2-49) by $C_p T_s$ and limit the discussion to isentropic barrel flow ($T < T^*$, $X_s < X_{s\ sonic}$) and

$$\theta_c = \theta_e + \frac{\gamma - 1}{2} V_e^2 \qquad (2\text{-}50)$$

and from Equation (2-8) and the fact that $X = V^2/2$,

$$\theta_c = 1 + (\gamma - 1) V^2 \qquad (2\text{-}51)$$

or

$$\theta_c = 1 + 2(\gamma - 1) X_s \qquad (2\text{-}52)$$

Using the isentropic condition,

$$\pi_c = \left[1 + 2(\gamma - 1) X_s\right]^{\gamma/\gamma - 1} \qquad (2\text{-}53)$$

The gas within the chamber is assumed to behave isentropically. Then

$$p_c v_c^{\gamma} = P_s v_o^{\gamma} \qquad (2\text{-}54)$$

where v_o is the specific volume in the chamber when the sabot is released. Let the initial charge of gas in the chamber be W_o. Then $v_o = \overline{V}_o/W_o$, $v_c = \overline{V}_c/w_c$, and

$$\frac{W_c}{M_s} = \frac{W_o}{M_s} - \int_o^t w \frac{dt}{M_s} \tag{2-55}$$

where the last term on the right is given by Equation (2-41). Then we see that

$$\pi_o = \frac{P_c}{P_s} = \left(\frac{\overline{V}_o}{\overline{V}_c} \frac{M_c}{W_o}\right)^{\gamma} = \left(\frac{\overline{V}_o}{\overline{V}_c}\right)^{\gamma} \left[1 - \frac{M_s}{W_o} \int_o^t \frac{w}{M_s} \, dt\right]^{\gamma} \tag{2-56}$$

or, using Equations (2-42) and (2-53)

$$\frac{\overline{V}_o}{\overline{V}_c} = \frac{\left[1 + (\gamma - 1)\, T^2\right]^{\frac{1}{\gamma - 1}}}{\left\{1 - \frac{M_s}{W_o}\left[\left(1 + \frac{\gamma - 1}{2}\, T^2\right)^{\frac{\gamma}{\gamma - 1}} - 1\right]\right\}} \tag{2-57}$$

2.2.5.2 Chamber Volume Behavior ($T > T^*$)

For the combined cycle the flow at the entrance is sonic and

$$\frac{T_c}{T_e} = \frac{\gamma + 1}{2} \tag{2-58}$$

and

$$\frac{P_c}{P_s} \cdot \frac{P_s}{P_e} = \left(\frac{\gamma + 1}{2}\right)^{\gamma/\gamma - 1} \tag{2-59}$$

or

$$\pi_c = \pi_e \left(\frac{\gamma + 1}{2}\right)^{\gamma/\gamma - 1} \tag{2-60}$$

The velocity at the entrance is given by Figure 2-3 and is equal to the sound speed hence we write Equation (2-60) as

$$\pi_c = \left[\theta_e \frac{\gamma + 1}{2}\right]^{\gamma/\gamma - 1} \tag{2-61}$$

$$\pi_c = \left[V_e^2 \frac{\gamma + 1}{2}\right]^{\frac{\gamma}{\gamma - 1}} \tag{2-62}$$

since $a'^2 = V^2 = \theta_e$. The term $\int_o^t w \frac{dt}{M_s}$ is obtained from Figure 2-4.

It should be noted at this point that the ratio $\frac{M_s}{W_o}$ appears as a free parameter and may be varied. Note that $\frac{2\gamma}{\gamma - 1}$ for $\gamma = 7/5$ is 7 and the chamber pressure grows rapidly with V_e. The behavior of $\overline{V}$ is then for $T > T^*$

$$\frac{\overline{V}_c}{\overline{V}_o} = \frac{1 - \frac{M_s}{W_o} \int_{T^*}^{T} \frac{w\, dt}{M_s} - \frac{M_s}{W_o} \int_o^{T^*} \frac{w}{M_s}\, dt}{\left[\overline{V}_c\right]^{\frac{2}{\gamma - 1}} \left(\frac{\gamma + 1}{2}\right)^{\frac{1}{\gamma - 1}}} \tag{2-63}$$

It is also of interest to compute the rate of chamber volume decrease. Then from Equation (2-56)

$$\frac{d\left(\frac{\overline{V}_c}{\overline{V}_o}\right)}{dT} = -\left(\frac{P_c}{P_s}\right)^{-\frac{1}{\gamma}} \frac{M_s}{W_o} \frac{W}{M_s} - \frac{1}{\gamma}\left(\frac{P_c}{P_s}\right)^{-\frac{1}{\gamma}} \frac{d\frac{P_c}{P_s}}{dT} \left[1 - \frac{M_s}{W_o} \int_o^t \frac{w}{M_s}\, dt\right] \tag{2-64}$$

and for $T < T^*$

$$\frac{P_c}{P_s} = \left|1 + (\gamma - 1)\, T^2\right|^{\gamma/\gamma - 1} \tag{2-65}$$

The variations of P_c/P_s is plotted in Figure 2-6.

Then

$$\frac{d\frac{P_c}{P_s}}{dT} = 2\,\gamma T\left[1 + (\gamma - 1)\,T^2\right]^{1/\gamma-1} \tag{2-66}$$

hence, for T < T*

$$\frac{d\frac{\nabla_c}{\nabla_o}}{dT} = -\left[1 + (\gamma - 1)\,T^2\right]^{-\frac{1}{\gamma-1}}\frac{M_s}{W}\frac{W}{M_s}$$

$$- 2T\frac{\overline{\nabla}_c}{\overline{\nabla}_o}\left[1 + (\gamma - 1)\,T^2\right]^{\frac{2-\gamma}{\gamma-1}} \tag{2-67}$$

Equation (2-67) indicates that the rate of volume decrease must begin at zero and increase thereafter. This behavior also is apparent in Figure 2-7 which is a volume time history for two cases of $W_o/M_s = \infty$ and 7.5. The curves differ little except that the finite mass case terminates. Equation (2-67) holds for T < T*. The complete similarity - unsteady cycle volume behavior must be obtained from Equation (2-63) for T > T*. The fact that the rate of volume decrease begins at zero indicates a fundamental difficulty encountered in real two-stage light-gas guns, if these guns achieve their initial pressure, P_s, by compressing initially cold gas with a moving piston. For true constant base-pressure operation, this piston must follow the curves in Figure 2-7 by coming to a halt, then reaccelerating and finally slowing during the final stage. For a fixed geometry piston the volume history curve must be approximated by a single line starting at $\nabla_c/\nabla_o = 1$ and decreasing in an approximately linear fashion. This behavior is shown in Figure 2-8. Although not specifically mentioned by early authors, the tapered chamber to barrel transition section probably allows the rate of volume decrease to change at the end of the stroke. If the piston can be

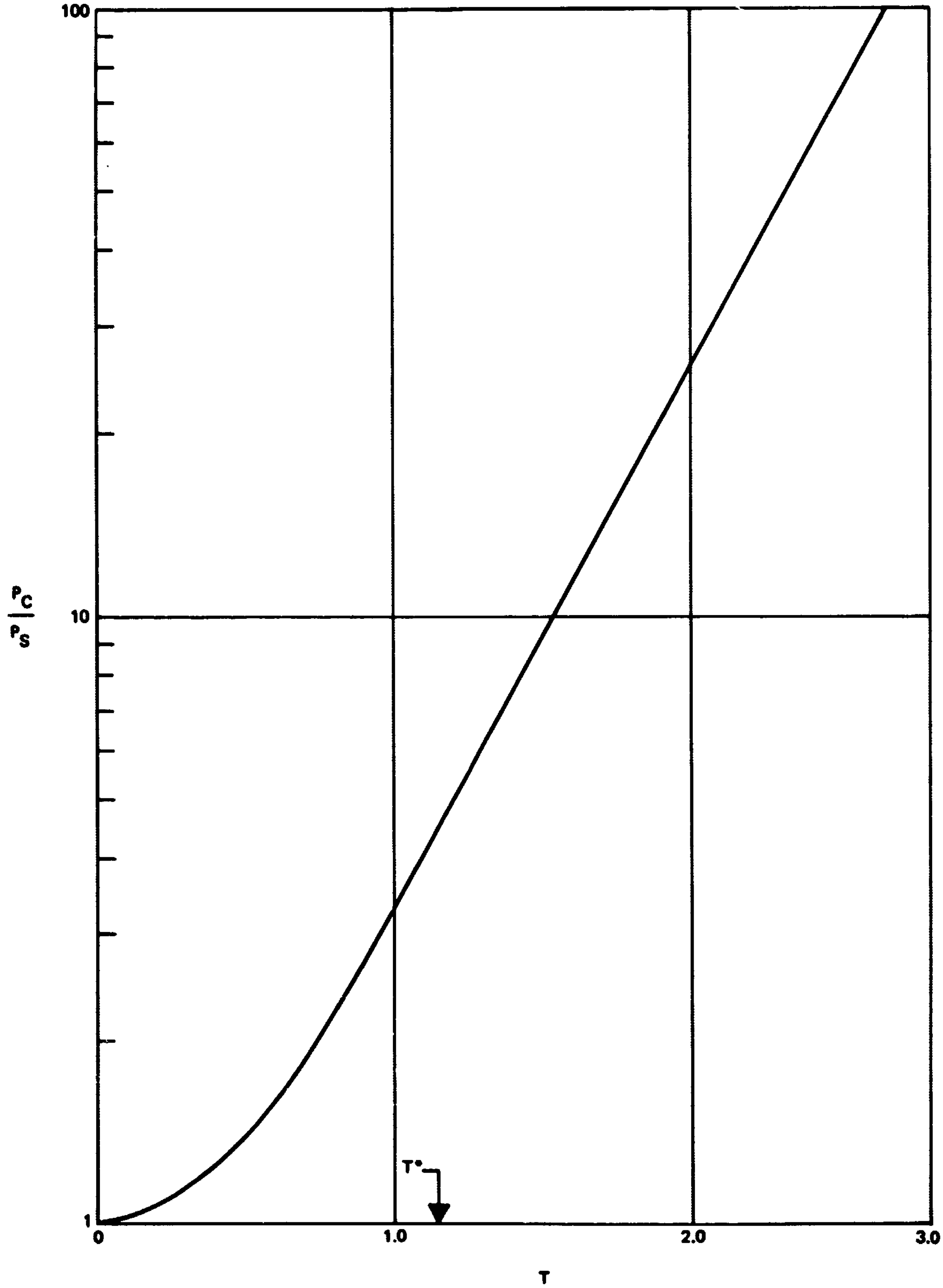

Figure 2-6. Chamber Pressure History for Similarity-Unsteady Cycle

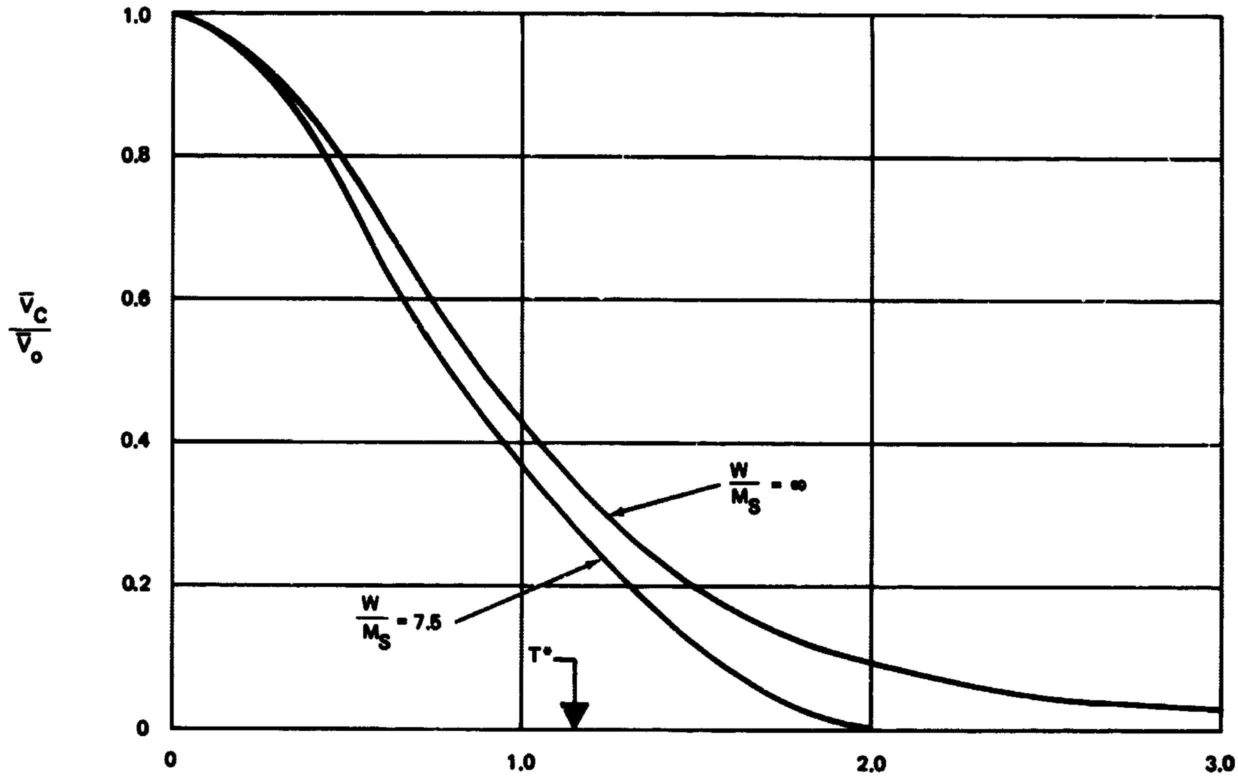

Figure 2-7. Chamber Volume Vs Time

constructed so that its forward face recedes for a nondimensional time T of about 0.15 and then stops collapsing and proceeds at a constant $\bar{V}_c/\bar{V}_o/dT$ of 0.589 until the taper is encountered at T of 1.5, a close approximation of the constant base-pressure cycle can be achieved. As yet, we have not prescribed the initial piston velocity. This can be obtained and the initial gas loading is known.

The base pressure, P_s, and temperature, T_s, are determined by structural limitations on the sabot. If a maximum value of T_s and P_s are selected as well as the final sabot velocity, the initial chamber conditions can be determined. If the gas in the chamber is compressed isentropically from room temperature we have

$$P_i = P_s (T_i/T_s)^{\gamma/\gamma - 1} \quad (2\text{-}68)$$

The minimum mass of gas in the chamber can be obtained from Figure 2-4 for a given V (V = T) and using the ideal gas law

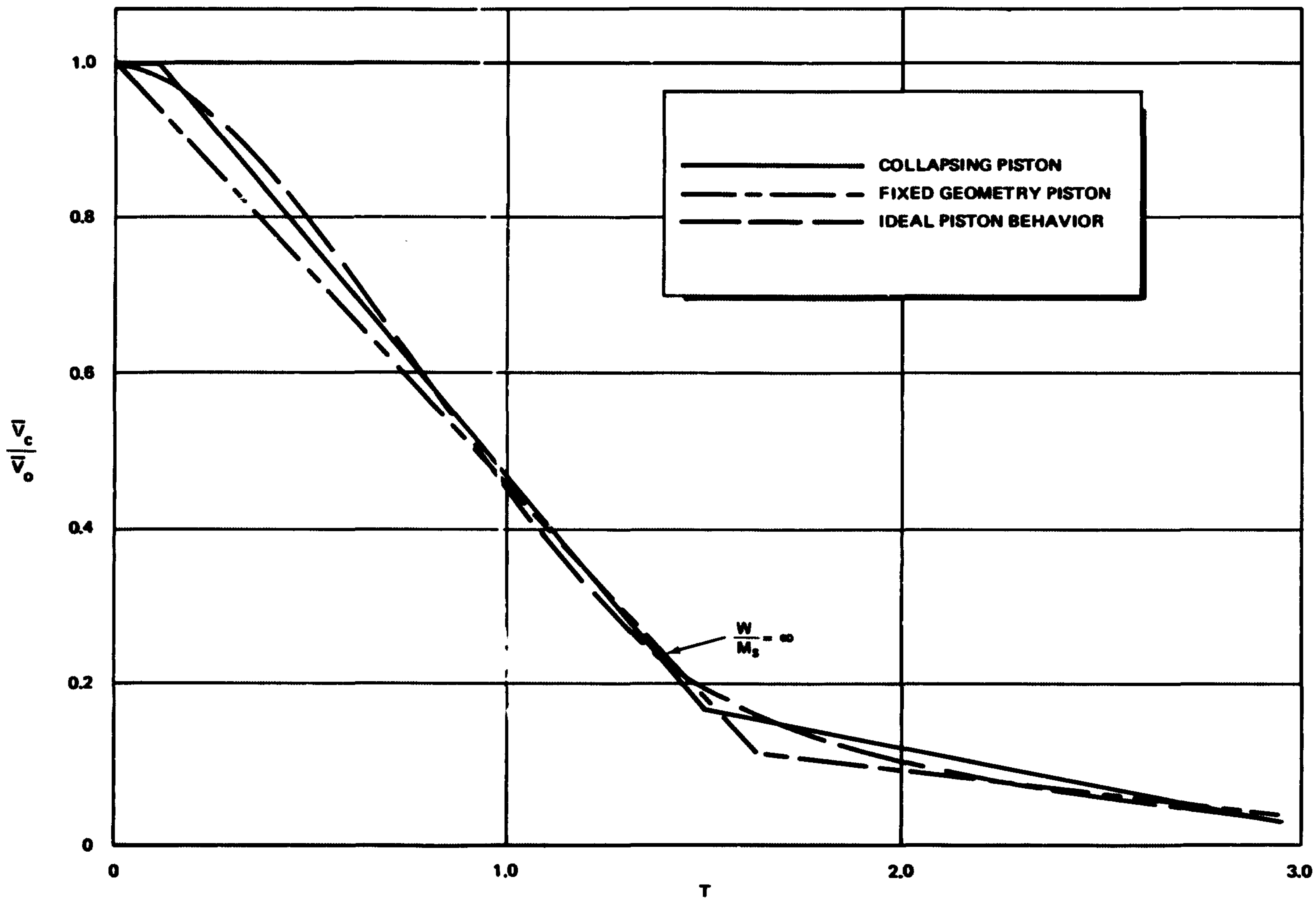

Figure 2-8. Approximate Chamber Volume Vs Time

$$P_i \overline{V}_i = W R T_i \tag{2-69}$$

Then we have

$$\overline{V}_i = \frac{WRT_i}{P_i} \tag{2-70}$$

The chamber volume at the release of the sabot is

$$\overline{V}_o = \overline{V}_i \left(\frac{T_i}{T_s}\right)^{\frac{1}{\gamma - 1}} \tag{2-71}$$

The required piston velocity is obtained from the requirement that d $\overline{V}_i/\overline{V}_o/dT$ be -0. 589. Then, since

$$\frac{d\,\overline{V}_c}{dt} = -U_p A_c \tag{2-72}$$

or

$$\frac{d\,\overline{V}_c/\overline{V}_o}{dT} = -\frac{U_p A_c M_s C_s}{\overline{V}_o P_s A_s} , \tag{2-73}$$

$d(\overline{V}_c/\overline{V}_o)/dT$ is -0. 589.

All terms except U_p are known. When U_p is found, the distance of front face recession is

$$L = U_p \cdot t_r \tag{2-74}$$

where

$$t_r = T_r \cdot \frac{M_s}{P_s A_s} \tag{2-75}$$

and

$$T_r \sim 0.15$$

Table 2-1 contains some typical calculations.

Table 2-1

2 IN. PUMP TUBE, 5/16 IN. BARREL

	Terminal Velocity (fps)			
	35,000	40,000	45,000	50,000
Base Pressure (P_s)	8,000	8,000	8,000	8,000
Base Temperature (°R)	2,870	2,870	2,870	2,870
Initial Temperature (°R)	540	540	540	540
Model Mass (gm)	0.2	0.2	0.2	0.2
Gas Mass, W (gm)	1.25	1.90	2.56	3.56
Pump Tube Length (ft)	6.9	23.9	31.8	44.3
Diaphragm Burst Length (in.)	2.82	4.33	5.76	8.03
Crush Length (in.)	0.252	0.382	0.515	0.719
Nontaper Length (in.)	2.26	3.84	4.62	6.44
Initial Pump Gas Pressure (psi)	23.2	23.2	23.2	23.2
Barrel Length (ft)	13.5	17.7	-	-
Pump Piston Speed (ft/sec)	625	961	1,280	1,780
Maximum Pump Pressure (psi)	170,000	256,000	384,000	576,000

PRECEDING PAGE BLANK NOT FILMED.

Section 3
DESCRIPTION OF EXPERIMENTAL APPARATUS

3.1 BALLISTIC RANGE A

The DAL Ballistic Range A is a two-stage light-gas gun coupled to a blast receiver, an instrument section, and an impact chamber. A discussion of each component of the A range follows, beginning with the powder chamber and ending down range at the impact chamber. Figure 3-1 shows the general arrangement of the DAL Ballistic Range A.

3.1.1 Powder Chamber

The A-Gun powder chamber is a thick-walled cylindrical high-pressure vessel with an inside diameter of 4.25 in. and 11.5-in. long. This gives an internal volume of approximately 163 cu in. A central rod supports the powder bag, a muslin container for the gun-powder and the initiating squibs. Electrical connectors pass through the breech plug providing a trigger circuit to fire the gun.

3.1.2 Pump Tube

Two interchangeable pump tubes are available with the A-Range. These tubes are identical except for inside diameter. The larger of the two has a 2-in. ID, the other a 1.5-in. ID. Both tubes are heavy-wall high-pressure tubes 20-ft long. At the upstream end these tubes have provision for installing a Lexan diaphragm to separate the powder chamber from the pump tube. The strength of the diaphragm helps control the powder chamber combustion pressure. There is a provision in both pump tubes for measuring the piston velocity by using a shorting pin technique. Both pump tubes share a common purge and gas-fill system. Connector flanges are common to both pump tubes.

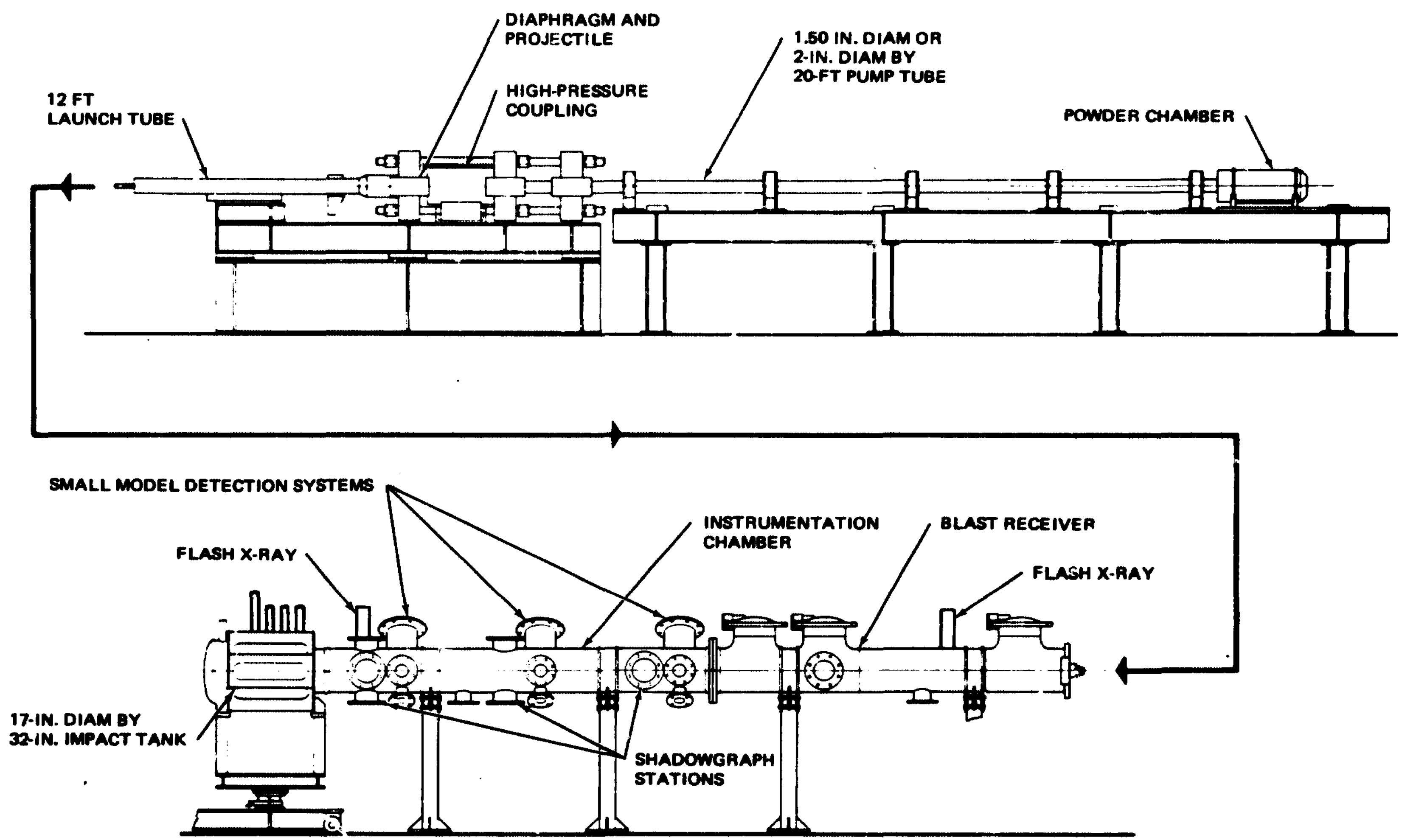

Figure 3-1. Light-Gas Gun--Ballistic Range A

3.1.3 Taper Section

Two interchangeable high-pressure taper sections are available for A-gun use. These taper sections match the corresponding 1.5- and 2-in. ID pump tubes. The larger 2-in. ID taper section is made of two individual pieces. The two-piece feature facilitates piston removal after a shot. Both taper sections have a liner insert in the high pressure region. When the interior of the high pressure region erodes beyond use, the liner insert is machined out and a new one installed. This liner-insert feature eliminates replacement of the entire taper section as the erosion progresses. Both taper sections have a converging conical ID in the high pressure region. The apex or the converging cone terminates at an ID of .375 in. There is provision at the downstream end of the taper section for a high pressure diaphragm. The bursting strength of this diaphragm is the major control on model acceleration.

3.1.4 Launch Tube

The DAL A-Gun uses a split-clamp-and-liner configured launch tube. New liners may be installed by unbolting the halves of the split clamp. This provides a relatively easy way to change launch tube diameter and also to replace eroded launch tubes. The launch tube ID can be varied from .2 in. to .375 in. depending upon which liner is used. Nominal launch tube length is 12 ft.

3.1.5 Blast Receiver

The A-Range blast receiver is made of 12-in. nominal diameter standard pipe. The blast receiver is approximately 9 ft long. Access to the inside of the blast receiver is through three 12-in. dia hinged closures. Instrumentation ports are provided at two stations in the blast receiver. One station is nominally used for flash X-ray and the other is used for a phototube pickup.

3.1.6 Instrumentation Section

The instrumentation section is fabricated from 12 in. nominal diameter standard pipe. The instrumentation section is approximately 9 ft long. There are six instrumentation stations within this section. These stations will accommodate 3 X-ray stations, 3 photo-tube model detector stations, and 2 shadowgraph stations. All instrumentation ports are fabricated from standard pipe flanges.

3.1.7 Impact Chamber

The impact chamber is an octagonal tank of approximately 18 in. dia and 35 in. long. Windows are fitted to each of the flats of the impact chamber wall. The windows are used for X-ray or optical study of target impact. The impact tank is connected to the instrument section with a quick-disconnect coupling. This coupling and a hinged closure at the downstream end of the impact chamber allow easy access to the target. Vacuum connections on the impact chamber provide a means of evacuating the impact chamber, instrument section, and blast receiver. A thick removable catcher is fitted to the downstream end of the impact chamber to stop the model flight.

3.2 RANGE "A" INSTRUMENTATION

3.2.1 Model Detection System

The range "A" instrument section contains three model detection stations spaced at intervals of 3.5 ft. A set of 6-in. dia windows immediately downstream from each model detection station provide access to the flight corridor for optical or radiographic instrumentation. For this particular test, flash X-ray was positioned at stations one and three to provide accurate velocity measurement and model integrity information.

The model detectors are electro optical devices that sense light from the luminous gas cap, when present, or from reflected light supplied by an auxiliary light screen. A photomultiplier views the model corridor through an optical system that limits sensitivity to a region 1/4-in. thick across the flight path. As the projectile crosses this 1/4-in. screen, light from the projectile reaches the photomultiplier, generating an electrical pulse. This pulse passes through a wideband line-matching amplifier and then on to the control room. Position accuracy of the system is ±1/4-in., and the rise time of the electronics is 50 nanoseconds. Figure 3-2 shows a typical record of the outputs of the model detection system

3.2.2 Flash X-ray System

Radiographs at stations one and three are accomplished with field-emission type flash X-ray equipment operating at 105 kv with a duration of 70 ns. Film casettes are placed against the window on one side of the instrument

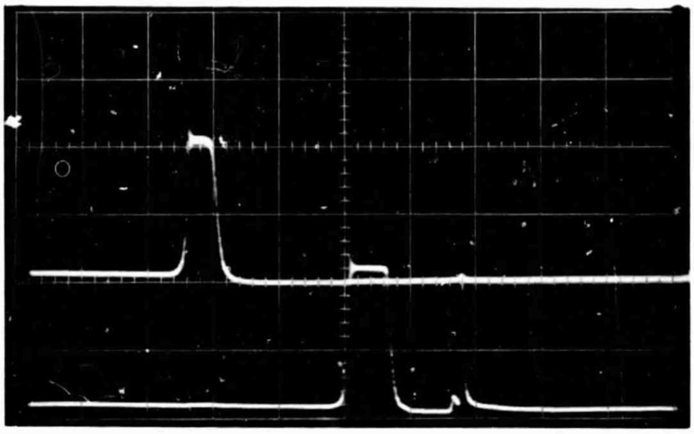

RUN NO. B42-23
SWEEP SPEED 50μ SEC/CM
DETECTOR SPACING 3.5 FT
PROJECTILE VELOCITY = 27,500 FT/SEC

Figure 3-2. Oscilloscope Record of Model Detection System

section, with an X-ray head at the center of the window opposite, and spaced away two feet. A reference line on the X-ray film serves as a position reference (Figure 3-3 shows typical X-ray record).

X-ray triggering is accomplished by the pulse from the adjacent model detector via a delay unit which delays the triggering signal the proper number of microseconds to allow the projectile to travel from the model detector to the center of the X-ray viewing window (about 10 inches). The X-ray flash records on film the exact position of the projectile while an electronic time interval meter records the exact time of the flash (to ± 0.1 μsec). The duration of the flash is sufficiently short to stop the motion of the projectile which, at a speed of 30,000 fps, moves approximately .020 inches during the 70 nanosecond exposure.

The velocity of the projectile is determined by dividing the distance traveled (established from the X-ray films) by the elapsed time between the two exposures. The accuracy of these measurements is such that velocity is determined to ±0.2%.

3.2.3 Superducer

Progress in improving the performance of a light-gas gun would be enhanced if it were possible to measure the breech pressure during the complete launch cycle. To this end DAL designed and built a Superducer capable of linear response to 290,000 psi without damage. The device is basically a high-pressure tapered-seal fitting with two coaxial stems housing the quartz pressure sensing elements at the tip. This transducer was completed late in the program and installed on the gun for run No. 14. Pressures were higher than anticipated (above 300,000 psi) and the transducer failed internally during the launch. Within its intended range the device worked well.

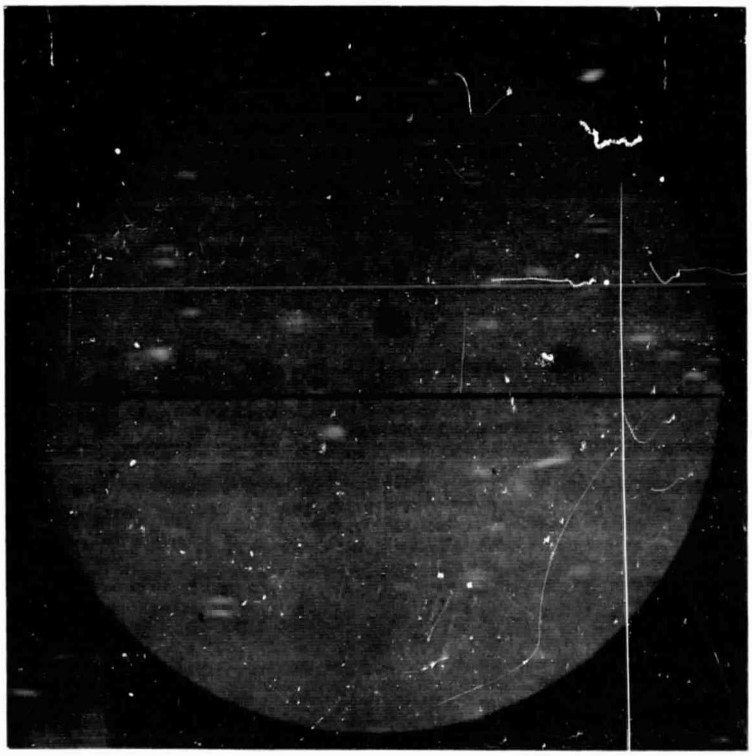

Figure 3-3. Typical X-Ray Record

Section 4
DISCUSSION OF EXPERIMENTAL PROGRAM

4.1 GENERAL DISCUSSION

In the conventional two-stage light-gas gun, the gas driving the projectile is brought to its final high pressure and high temperature through the use of a single moving piston. This piston travels down a pump tube containing a low-molecular-weight driver gas, such as hydrogen or helium, initially at low pressure. The piston compresses the gas raising both its temperature and pressure. Attached to the downstream end of the pump tube is a launch tube containing the projectile which is subsequently driven by this compressed gas.

Once the projectile moves down the launch tube, the pressure behind it will remain at a near constant level only if the pressure of the gas in the pump tube continues to increase at a certain rate. The rate must be properly adjusted for a given gun and projectile, otherwise, either the pressure behind the projectile will decrease, resulting in failure to achieve desired velocity, or the pressure may become too high, resulting in model and/or gun structural failure. Obviously, when the projectile is still near the breech, the pressure of the pump tube must rise slowly. Later, when the projectile is farther along the launch tube and is moving faster, the pressure must rise more rapidly. For a given piston kinetic energy, a light piston moves at a relatively high speed, such that the projectile will experience too high a pressure at the beginning of the launch cycle. This can be corrected somewhat by decreasing piston velocity and increasing piston mass, but then, although the model feels the correct pressure at the beginning, the piston will be stopped too quickly and the pressure behind the model will be too low at the far end of the barrel.

In the theory developed in Section 2, constant base-pressure launch cycle may be approximated if the chamber volume history can be produced as required by Figure 2-8. The requirement dictates the movement of the front end of the piston.

At the beginning of the launch cycle (immediately after the diaphragm rupture) the piston should have zero velocity. After the projectile is set into motion, the piston is required to travel at a given near-constant speed for a period as indicated in Figure 2-8. The history of piston deceleration on projectile velocity after the constant speed period is very small.

Figure 4-1 depicts a piston satisfying the above requirements. The operating principle is as follows: in place of the conventional, single, heavy piston used in two-stage light-gas gun operation, a variable-speed piston assembly is used. As the piston assembly travels down the pump tube, the gas pressure in front of the piston assembly continues to rise until the diaphragm at the breech ruptures and launching of the projectile commences. The shear disc assembly which pushes against the front section of the piston will then fail at a designed stress level along a controlled failure area. The failure of the shear disc temporarily disconnects the front piston from the rear one which comprises the majority of the total piston weight. A short time later, the rear piston catches up with the front piston to further compress the driving gas. Thus, the ideal piston time-position relationship can be approached.

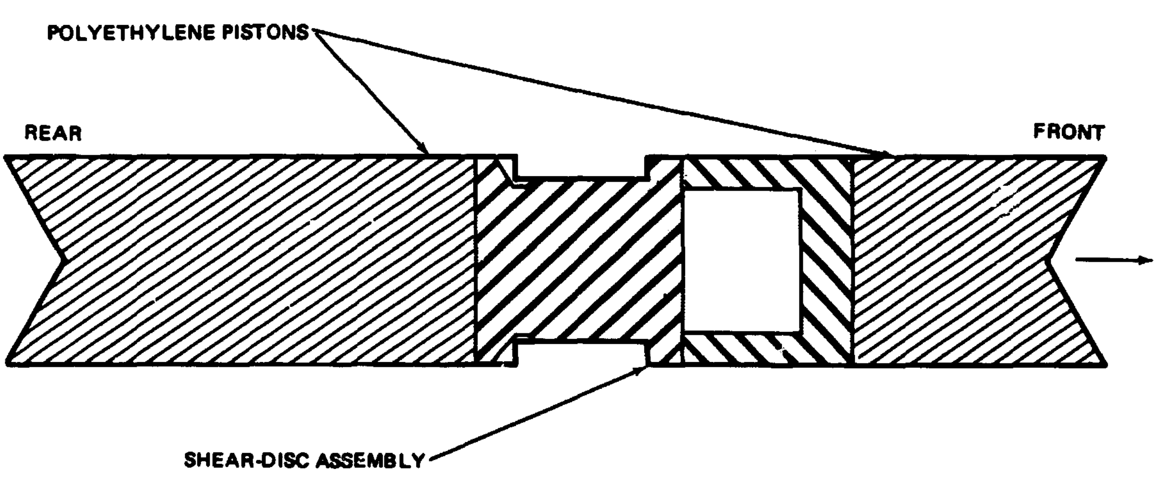

Figure 4-1. Piston Assembly With Typical Collapsible Mechanism

To illustrate the concept of a collapsible piston further, a family of hypothetical chamber pressure histories is shown in Figure 4-2. It can be shown for a given light-gas gun, projectile, and propellant the obtainable muzzle velocity is a function of the projectile base-pressure (which is directly related to the chamber pressure). The values identified in Figure 4-2 are believed to be typical in a two-stage light-gas gun operation.

Line 1 represents the reservoir pressure history of a constant projectile base pressure (12,000 psi) launch cycle. The muzzle velocity achieved is 23,000 fps. Line 2 is the pressure history of a non-constant base-pressure solid-piston shot. The peak pressure experienced by the projectile is 30,000 psi and the muzzle velocity is 31,000 fps. Line 3 represents a potentially maximum velocity solid-piston launch cycle of 40,000 fps. Characteristically, a sharp pressure spike occurs at the early part of this type of launch cycle. This spike can permanently damage the gun components as well as fracture the projectile.

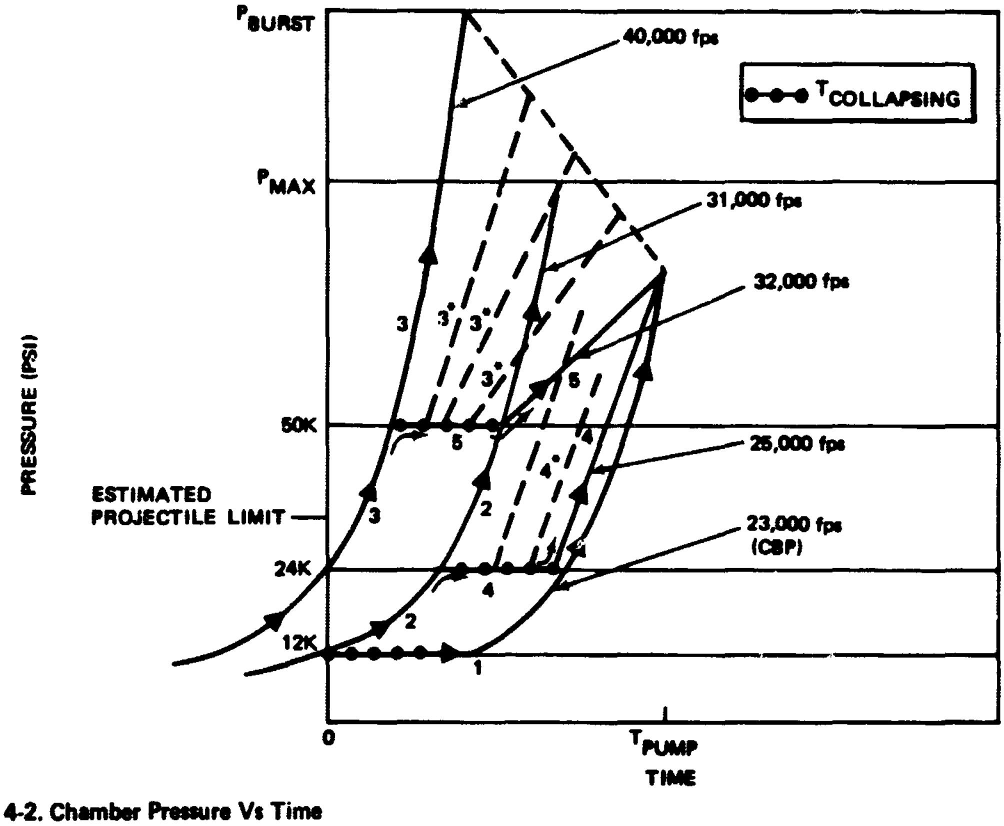

Figure 4-2. Chamber Pressure Vs Time

To minimize the pressure spike and yet retain a sufficiently high pressure of long duration in the chamber so that a high muzzle velocity can be achieved without damaging the gun, lines 4 and 5 must be followed. The level portions of the lines 4 and 5 show the effects of using a collapsing mechanism in the piston assemblies (Figure 4-1). In the above case the collapsing mechanism portions are made of aluminum glass-reinforced epoxy (Scotchply) and steel with the respective collapsing pressures at 24,000 psi, 20,000 psi, and 50,000 psi. Line 4 yields a muzzle velocity of 26,000 fps, line (5) yields 32,000 fps.

The dashed lines 3* and 4* in Figure 4-2 represent families of pressure histories for which various collapsing times are incorporated. The collapsing times decrease toward the left while the muzzle velocities increase toward 40,000 and 31,000 fps respectively.

The experimental program described in the following sections was specifically designed to verify the constant base-pressure launch-cycle and the cycles as indicated in Figure 4-2.

4.2 PISTON VELOCITY CALIBRATION

In order to control the experiment, piston velocities must be held within a close tolerance (±5 percent). Runs No. 1 through 8 (Table 4-1) were fired to calibrate the piston velocity under various loading conditions. After run No. 4 it was discovered that the piston, ballasted by a lead cylinder (3180 gm) had rebounded into the pump tube. This phenomena, coupled with a measured low muzzle-velocity, caused considerable concern.

In runs 4 through 8, lead slurries (wax plus lead pellets) were substituted for the lead cylinder. Although the muzzle velocities were still far below computed velocities, the piston rebounding was comparatively less than in the first three runs.

4.3 CONSTANT-PRESSURE LAUNCH-CYCLE

To verify the theory developed in Section 2, calculations similar to those tabulated in Table 2-1 were developed. The desired projectile velocity was 30,000 fps. Other loading parameters can be found in Table 4-1 (runs 9 through 12). The muzzle velocities in this series never exceeded 20,000 fps.

Table 4-1

SUMMARY OF TEST RESULTS

Run No.	Date	Launch Tube ID (in.)	Pump Tube ID (in.)	H_2 (psig)	Powder (gram)	Piston			Projectile					Test Objective	Comments
						Mass (gram)	Design	Velocity (fps)	Mass (gram)	Material	Length (in.)	Dia (in.)	Velocity (fps)		
1	10-8-69	0.517	2.00	50	150	454	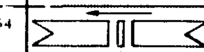	2,100	0.85	Polyethylene	0.259	0.517	24,000	• To shake down the new gun • To measure piston velocity	Projectile intact Piston velocity obtained
2	10-17-69	0.517	2.00	50	150	3,180	Same as Run No. 1	--	0.85	Polyethylene	0.259	0.517	15,000	• To calibrate projectile velocity with piston velocity • To calibrate piston velocity against gun powder	Only projectile velocity obtained No piston velocity
3	10-21-69	0.517	2.00	50	150	3,180	Same as Run No. 1	295	0.85	Polyethylene	0.259	0.517	14,500	Same as Run No. 2	Obtained all data
4	10-21-69	0.517	2.00	50	250	3,180	Same as Run No. 1	590	0.85	Polyethylene	0.259	0.517	16,700	Same as Run No. 2	Obtained all data Piston rebounded
5	10-23-69	0.517	2.00	50	350	3,180	Same as Run No. 1	1,390	0.85	Polyethylene	0.259	0.517	21,600	Same as Run No. 2	Obtained all data Taper section cracked near pressure-transducer mount
6	10-31-69	0.517	2.00	50	250	3,180		520	0.85	Polyethylene	0.259	0.517	16,700	• Same as Run No. 2 • To resolve the problem of piston rebound by adding wax to lead blast weight	Obtained all data Less piston rebound
7	11-6-69	0.517	2.00	50	300	3,180	Same as Run No. 6	1,280	0.85	Polyethylene	0.259	0.517	19,700	Same as Run. No. 6	Obtained all data Pressure-transducer mount cracked again
8	11-7-69	0.517	2.00	50	300	3,180	Same as Rur No. 6	1,225	0.85	Polyethylene	0.259	0.517	19,500	• Same as Run No. 6 • To checkout taper section integrity after repair	Obtained all data Taper section intact after run
9	11-17-69	0.312	2.00	15	230	3,180	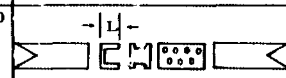 Collapse Distance, L = 0.25 in.	1,110	0.20	Polyethylene	0.312	0.161	17,500	To checkout theoretical constant base-pressure launch-cycle. Velocity objective: 30,000 fps	Low velocity suspected due to lead movement during pump cycle
10	11-18-69	0.312	2.00	15	230	3,180	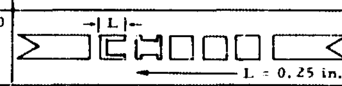	1,[illegible]	0.195	Polyethylene	0.312	0.161	16,300	• Same as Run No. 9 • To checkout effectiveness of brass ballast-weight	Piston rebounded and siezed in pump tube
11	11-21-69	0.312	2.00	30	230	3,180	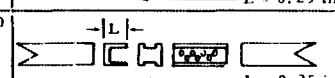	1,180	0.195	Polyethylene	0.312	0.161	17,300	• Same as Run No. 9 • Lead pieces and wax casted in polyethylene thin wall tube	Piston rebounded Pressure seal failed
12	11-25-69	0.312	2.00	15	230	3,180	Same as Run No. 11	1,190	0.195	Polyethylene	0.312	0.161	--	• Same as Run No. 9 • To determine cause of piston rebound • To checkout new pressure-seal design	Piston rebounded and seal failed again
13	11-26-69	0.312	2.00	15	180	454	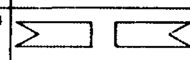	2,600	0.20	Polyethylene	0.319	0.161	26,000	To check gun performance with non-constant base-pressure driving mode. Objective: 28,000 fps	Taper section cracked.
14	1-14-70	0.385	2.00	50	200	1,100	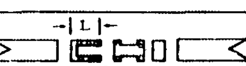 L = 1.0 in.	2,300	0.340	Polyethylene	0.385	0.190	27,000	To determine maximum-performance launch-cycle limits	All data obtained Piston rebounded
15	1-15-70	0.385	2.00	40	200	1,[illegible]	Same as Run No. 14 L = 0.75 in.	2,400	0.340	Polyethylene	0.385	0.190	27,500	Same as Run No. 14	All data obtained Less piston rebound
16	1-19-70	0.385	2.00	20	240	1,100	Same as Run No. 14 L = 0.5 in.	2,600	0.340	Polyethylene	0.385	0.190	28,500	Same as Run [illegible]	All data obtained [illegible]

FOLDOUT FRAME /

14	1-14-70	0.385	2.00	50	200	1,100	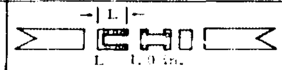 L = 1.0 in.	2,300	0.340	Polyethylene	0.385	0.190	27,000	To determine max. num-performance launch-cycle limits	All data obtained Piston rebounded
15	1-15-70	0.385	2.00	40	200	1,100	Same as Run No. 14 L = 0.75 in.	2,400	0.340	Polyethylene	0.385	0.190	27,500	Same as Run No. 14	All data obtained Less piston rebound
16	1-19-70	0.385	2.00	20	240	1,100	Same as Run No. 14 L = 0.5 in.	2,600	0.340	Polyethylene	0.385	0.190	28,500	Same as Run No. 14	All data obtained Piston rebounded
17	1-20-70	0.385	2.00	15	180	716	Same as Run No. 14 L = 0.25 in.	2,800	0.340	Polyethylene	0.385	0.190	31,000	Same as Run No. 14	All data obtained Piston rebounded
18	1-28-70	0.385	2.00	15	180	716	Same as Run No. 14 L = 0.25 in.	2,850	0.340	Polyethylene	0.385	0.190	31,500	Same as Run No. 14	All data obtained Piston rebounded High-pressure seal broke
19	1-29-70	0.385	2.00	15	200	900	Same as Run No. 14 L = 0.25 in.	2,700	0.340	Polyethylene	0.385	0.190	--	• Same as Run No. 14 • To checkout 30,000 psi break diaphragm	Model broke in launch tube
20	2-13-70	0.385	2.00	15	180	704	Same as Run No. 14 L = 0.25 in.	2,800	0.340	Polyethylene	0.385	0.190	31,000	• Same as Run No. 14 • To checkout collapsible mechanism with machined groves	All data obtained Piston rebound reduced
21	3-6-70	0.318	1.5	20	140	310	Same as Run No. 1	--	0.190	Polyethylene	0.320	0.150	--	To checkout new pump tubes	Model broke
22	3-7-70	0.318	1.5	20	140	310	Same as Run No. 1	2,340	0.190	Polyethylene	0.320	0.150	28,000	Same as Run No. 21	Gun operated satisfactorily
23	3-9-70	0.318	1.5	20	140	325	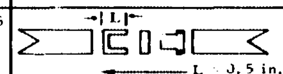 L = 0.5 in.	2,370	0.190	Polyethylene	0.320	0.150	27,500	To checkout effect of Scotchply collapsible mechanism	All data obtained No piston rebound
24	3-10-70	0.323	1.5	20	180	325	Same as Run No. 23	2,690	0.193	Polyethylene	0.323	0.150	27,000	Same as Run No. 23	All data obtained No rebound
25	3-10-70	0.324	1.5	30	180	325	Same as Run No. 23	2,680	0.193	Polyethylene	0.324	0.150	26,000	Same as Run No. 23	All data obtained No piston rebound Collapsible mechanism shattered
26	3-11-70	0.326	1.5	20	180	325	Same as Run No. 1	2,660	0.193	Polyethylene	0.326		31,500	To attempt higher speed limit	All data obtained No piston rebound
27	3-12-70	0.326	1.5	20	200	344	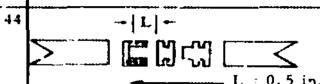 L = 0.5 in.	2,700	0.193	Polyethylene	0.325	0.150	27,500	To evaluate slotted aluminum collapsible mechanism design	All data obtained No piston rebound
28	3-20-70	0.326	1.5	20	200	455	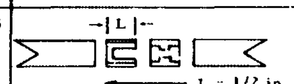 L = 1/2 in.	2,380	0.193	Polyethylene	0.326	0.150	--	To evaluate 17-4 PH collapsible-mechanism design; 30,000 psi diaphragm	Model broke during launch, possibly due to high diaphragm pressure
29	3-23-70	0.326	1.5	20	200	455	Same as Run No. 28	2,420	0.193	Polyethylene	0.326	0.150	27,500	Same as Run No. 28	All data obtained after launch tube honed
30	3-25-70	0.326	1.5	20	240	455	Same as Run No. 28	2,600	0.193	Polyethylene	0.326	0.150	--	Same as Run No. 28	Model, seals of taper section, and diaphragm all broke
31	3-31-70	0.312	1.5	20	180	310	Same as Run No. 1	2,640	0.20	Polyethylene	0.312	0.150	26,800	To checkout and calibrate temporary repair of taper section and 20,000 psi break diaphragm	Low performance compared with Run No. 26 due to local enlargement in taper section
32	4-1-70	0.312	1.5	20	180	310	Same as Run No. 1	2,540	0.20	Polyethylene	0.312	0.150	--	Same as Run No. 31	Model broke during launch
33	4-2-70	0.327	1.5	20	180	310	Same as Run No. 1	2,680	0.20	Polyethylene	0.327	0.150	27,300	To checkout new launch tube	All data obtained Model rotated
34	4-3-70	0.327	1.5	20	180	310	Same as Run No. 1	2,670	0.305	Lexan	0.327	0.200	26,300	To checkout model design and effect of model mass	All data obtained
35	4-3-70	0.327	1.5	10	200	455	Same as Run No. 1	2,370	0.23	Lexan	0.327	0.200	29,000	To evaluate piston mass effect	All data obtained
36	4-6-70	0.327	1.5	10	240	455	Same as Run No. 28	2,630	0.23	Lexan	0.327	0.200	26,200	To checkout 17-4 collapsible-mechanism with thin diaphragm	All data obtained Model partially broke
37	4-10-70	0.327	1.5	10	140	230	Same as Run No. 13	2,700	0.23	Lexan	0.327	0.200	24,600	To check piston mass/projectile velocity relationship	All data obtained
38	4-13-70	0.327	1.5	10	180	310	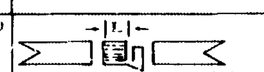 L = 1.0 in.	2,700	0.23	Lexan	0.327	0.200	26,500	To check plastic column collapsible mechanism	All data obtained
39	4-13-70	0.327	1.5	20	180	310	Same as Run No. 38	2,670	0.23	Lexan	0.327	0.200	--	To check H_2 and velocity relationship	Model tumbled off trajectory
40	4-14-70	0.334	1.5	30	200	310	Same as Run No. 38	2,740	0.23	Lexan	0.334	0.150	28,000	To check effect of	Model tumbled

FOLDOUT FRAME 2

27	3-12-70	0.326	1.5	20	200	344	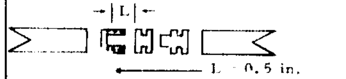 L = 0.5 in.	2,700	0.193	Polyethylene	0.326	0.150	27,500	To evaluate slotted aluminum collapsible mechanism design	All data obtained No piston rebound
28	3-20-70	0.326	1.5	20	200	455	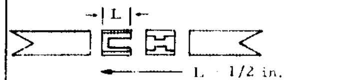 L = 1/2 in.	2,380	0.193	Polyethylene	0.326	0.150	--	To evaluate 17-4 PH collapsible-mechanism design; 30,000 psi diaphragm	Model broke during launch, possibly due to high diaphragm pressure
29	3-23-70	0.326	1.5	20	200	455	Same as Run No. 28	2,420	0.193	Polyethylene	0.326	0.150	27,500	Same as Run No. 28	All data obtained after launch tube honed
30	3-25-70	0.326	1.5	20	240	455	Same as Run No. 28	2,600	0.193	Polyethylene	0.326	0.150	--	Same as Run No. 28	Model, seals of taper section, and diaphragm all broke
31	3-31-70	0.312	1.5	20	180	310	Same as Run No. 1	2,640	0.20	Polyethylene	0.312	0.150	26,800	To checkout and calibrate temporary repair of taper section and 20,000 psi break diaphragm	Low performance compared with Run No. 26 due to local enlargement in taper section
32	4-1-70	0.312	1.5	20	180	310	Same as Run No. 1	2,540	0.20	Polyethylene	0.312	0.150	--	Same as Run No. 31	Model broke during launch
33	4-2-70	0.327	1.5	20	180	310	Same as Run No. 1	2,680	0.20	Polyethylene	0.327	0.150	27,300	To checkout new launch tube	All data obtained Model rotated
34	4-3-70	0.327	1.5	20	180	310	Same as Run No. 1	2,670	0.305	Lexan	0.327	0.200	26,300	To checkout model design and effect of model mass	All data obtained
35	4-3-70	0.327	1.5	10	200	455	Same as Run No. 1	2,370	0.23	Lexan	0.327	0.200	29,000	To evaluate piston mass effect	All data obtained
36	4-6-70	0.327	1.5	10	240	455	Same as Run No. 28	2,630	0.23	Lexan	0.327	0.200	26,200	To checkout 17-4 collapsible-mechanism with thin diaphragm	All data obtained Model partially broke
37	4-10-70	0.327	1.5	10	140	230	Same as Run No. 13	2,700	0.23	Lexan	0.327	0.200	24,600	To check piston mass/projectile velocity relationship	All data obtained
38	4-13-70	0.327	1.5	10	180	310	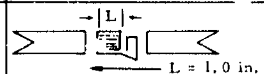 L = 1.0 in.	2,700	0.23	Lexan	0.327	0.200	26,500	To check plastic column collapsible mechanism	All data obtained
39	4-15-70	0.327	1.5	20	180	310	Same as Run No. 38	2,670	0.23	Lexan	0.327	0.200	--	To check H_2 and velocity relationship	Model tumbled off trajectory
40	4-14-70	0.334	1.5	20	200	310	Same as Run No. 38 Except column length was 0.5 in.	2,740	0.23	Lexan	0.334	0.150	28,000	To check effect of 0.5 in. column	Model tumbled
41	4-20-70	0.316	1.5	20	180	310	Same as Run No. 1	2,660	0.2	Lexan	0.316	0.150	27,800	To checkout new launch tube	Good launch, leak at diaphragm holder
42	4-21-70	0.316	1.5	20	180	310	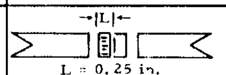 L = 0.25 in.	2,720	0.2	Lexan	0.316	0.150	26,500	• To fix seal • To reduce column distance to 0.25 in.	Model tumbled slightly, still leaked
43	4-21-70	0.316	1.5	10	180	310	Same as Run No. 42	2,620	0.20	Lexan	0.316	0.150	28,000	To fix leak	Data obtained Model slightly tumbled
44	4-22-70	0.316	1.5	10	180	310	Same as Run No. 42	2,710	0.27	Lexan	0.316	0.150	28,200	To fix diaphragm leak	Found leak due to uneven pressure against diaphragm
45	4-23-70	0.316	1.5	10	180	310	Same as Run No. 42	2,700	0.27	Lexan	0.316	0.150	--	To evaluate double-seal design	No leak-instrument failed to record
46	4-24-70	0.317	1.5	10	200	310	Same as Run No. 38	2,800	0.21	Lexan	0.317	0.150	29,200	To determine powder velocity relationship, 1-in. column length	All data obtained
47	4-24-70	0.317	1.5	20	200	310	Same as Run No. 38	2,830	0.21	Lexan	0.317	0.150	20,800	To determine pre-charge H_2 and muzzle velocity relationship	Blast lead punched through front piston
48	4-27-70	0.317	1.5	20	240	455	Same as Run No. 42	2,660	0.23	Lexan	0.317	0.150	30,500	To attempt higher velocity	All data obtained
49	4-28-70	0.317	1.5	10	280	455	Same as Run No. 42	2,840	0.23	Lexan	0.317	0.150	31,000	To attempt higher velocity	All data obtained
50	4-29-70	0.321	1.5	10	280	310	Same as Run No. 42	3,190	0.23	Lexan	0.321	0.150	32,600	To attempt higher velocity	All data obtained
51	4-29-70	0.321	1.5	5	280	250	Same as Run No. 13	3,580	0.23	Lexan	0.321	0.150	--	To attempt maximum velocity	Model broke - maximum acceleration exceeded
52	4-30-70	0.321	1.5	10	280	250	Same as Run No. 13	3,600		Lexan	0.321	0.150	--	Same as Run No. 51	Model broke - taper section cracked

Range pressure for all runs = 11 Torr
Launch tube length for all runs = 12 ft
Diaphragm rupture pressure = 18,000 psi (except Run No. 28)

The piston rebounding became more pronounced than in the calibration runs. The only difference in piston design was that an aluminum collapsible-mechanism (0.25-in. travel, 12,000 psi fail load) similar to the design in Figure 4-1 was used. One of the collapsible mechanisms recovered after the run is shown in Figure 4-3.

The pistons that rebound into the pump tubes required firing another piston to shoot it out. The galling was quite severe.

At this point it was realized that the friction between the piston and pump tube wall could not be ignored as assumed in the theory. The friction force became great early in the launch cycle when the hydrogen pressure built to more than 20,000 psi. Close examination of the inside walls of the high-pressure components (pump tube and taper section) revealed a thin film deposit of piston material after each run. This suggested that the wall friction actually sheared off the outer layer of the piston like the molting action of a snake.

A rough calculation, based on the shear stress of the piston materials, showed the piston wasted a significant portion of its energy in overcoming the launch-cycle friction.

A slow, lengthy (large shear-area) and heavy piston, as required by the constant base-pressure launch-cycle, would prematurely stop. As a result, the base pressure of the model started at the correct level, but declined very rapidly as the piston fell off from the theoretical trajectory. The remaining high-pressure hydrogen in the chamber forced the piston back into the pump tube.

Since the relationship of piston friction and gun-loading conditions is unknown, the pursuance of the constant base-pressure cycle was terminated in favor of the maximum-performance cycle discussed in Section 4.1 and shown in Figure 4-2.

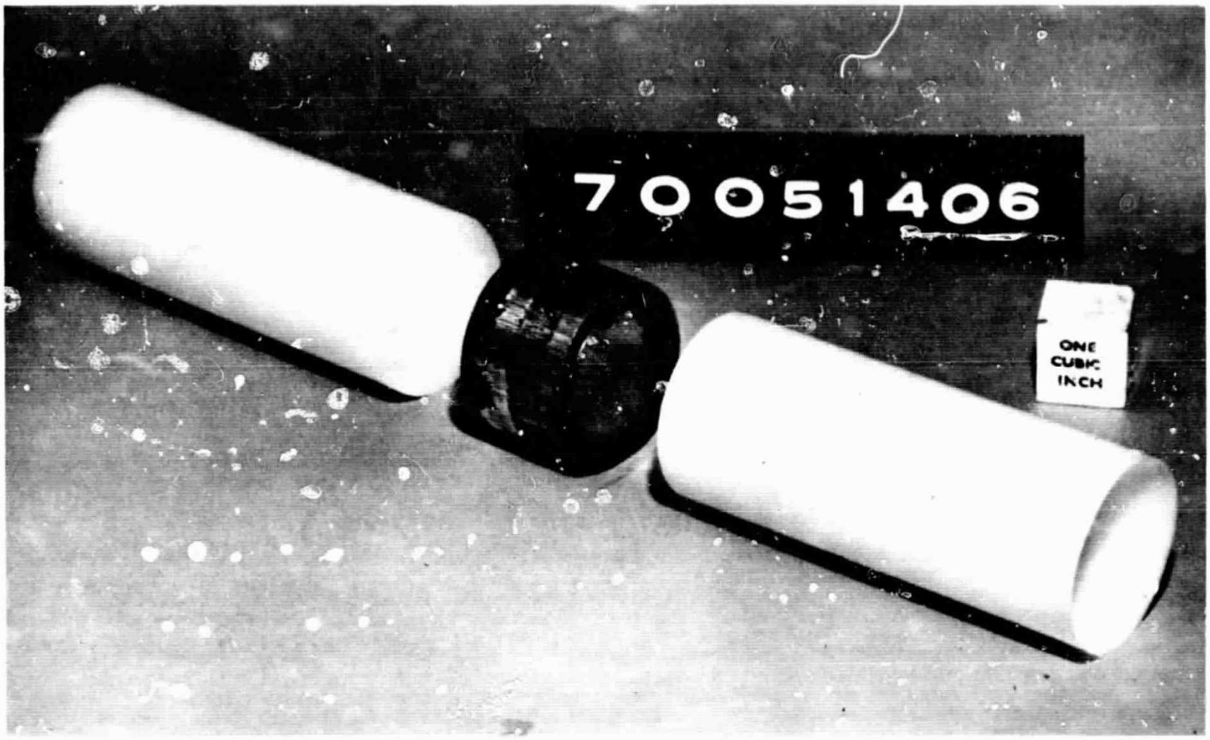

Figure 4-3. Plain Collapsing Mechanism Recovered After Run

4.4 MAXIMUM-PERFORMANCE LAUNCH-CYCLE

Since there was no simple theory to govern the maximum-performance launch-cycle, a family of empirical curves based on the available information was generated. Figure 4-2 presents one of the typical families of curves. To verify these curves experimentally, two alternative approaches can be taken. For example:

A. The gun may be loaded to follow the curve 2 without employing any collapsible mechanism on the first attempt. The subsequent runs will incorporate collapsible mechanisms of various shear loads and collapse distances to map out curves 4*.

B. On the first attempt the gun may be loaded with a collapsible mechanism of sufficient shear strength and maximum collapse-distance so as to follow curve 5. The subsequent runs would incorporate identical loading parameters except for the collapse distances. This procedure is particularly preferred for runs near gun-rupture loading conditions.

In this program the A approach was used for runs of moderate loading conditions, and the B approach for maximum loading conditions.

4.4.1 Aluminum Collapsing Mechanism

It was established in the constant base-pressure launch-cycle tests that the friction between the plain-aluminum collapsing-mechanism and the walls of the high-pressure components was so great that the piston always retarded prematurely. As a result, the aluminum collapsing-mechanisms were modified as shown in Figure 4-4. The outer rings sheared off when the friction on the wall became great, leaving the center core to continue compressing hydrogen in the chamber at the desired rate. 7075-T6 Aluminum was used for the collpasing mechanism with the shear disc designed to fail when chamber hydrogen pressure reached 24,000 psi. Two series of tests were conducted; the first, runs 14 through 20 (Table 4-1), with a 2-in. ID pump tube and 0.385-in. ID launch tube; the second series, runs No. 26 and 27 (Table 4-1), with a 1.50-in. ID pump tube and 0.326-in. ID launch tube.

4.4.2 Glass-Reinforced Epoxy (Scotchply) Collapsing-Mechanism

Scotchply has good shear strength due to the orientation of its glass filaments. The friction coefficient is lower than aluminum under high temperature.

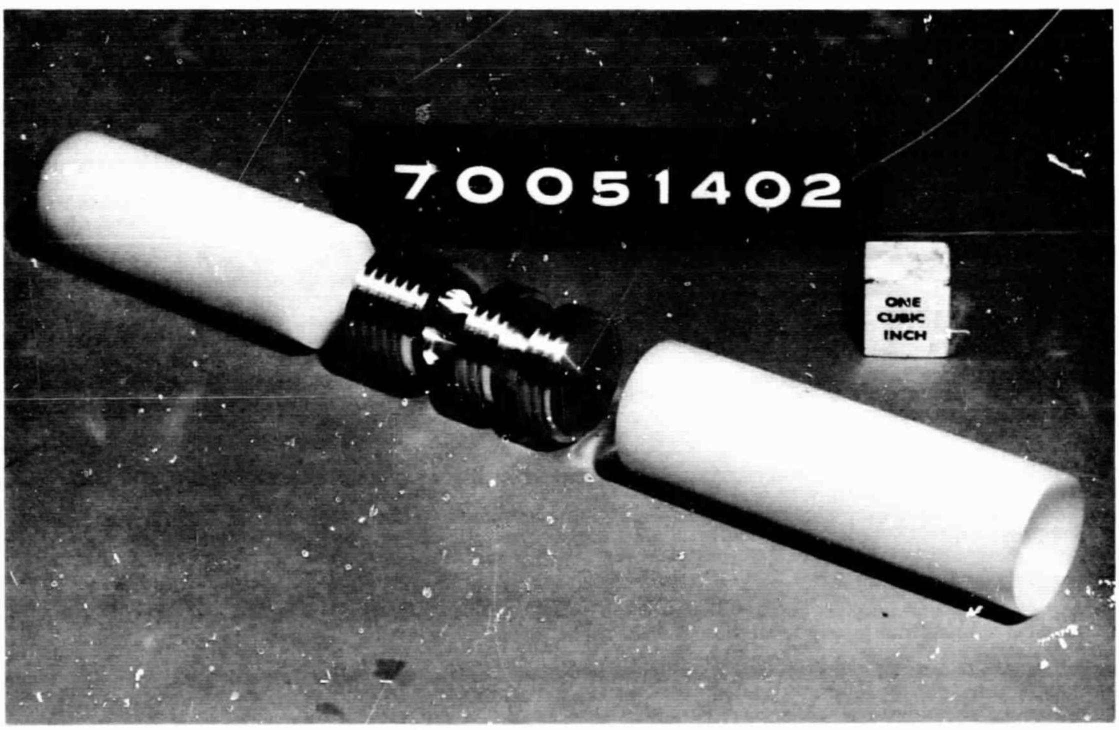

Figure 4-4. Modified Aluminum Collapsing-Mechanism

Hence, runs No. 23, 24, and 25 were devoted to evaluating the material as a candidate for the collapsing mechanism (shear disc designed to fail at 20,000 psi) (Figure 4-5). No piston rebound was observed during any of the three runs, thus verifying the low-friction characteristic assumption. However, severe material delamination of the mechanisms was noticed.

4.4.3 17-4 PH Stainless-Steel Collapsing-Mechanism

To meet design requirements for the shear disc to fail at 50,000 psi chamber pressure, high strength steel must be employed. 17-4 PH stainless steel, heat-treated to 900 H, was chosen for its strength. However, the metal was too hard for the gun components so that ring-groove design similar to the aluminum collapsing-mechanism was not feasible. To prevent scoring, Lexan sleeves were threaded over the 17-4 PH stainless steel mechanism (Figure 4-6). Runs No. 28, 29 and 30 (Table 4-1) were made to evaluate the effectiveness of this design. It was found that the high-shear design performance approaches that of the piston with no collapsing mechanism. This is to be expected.

4.4.4 Variable Recessing-Rate Collapsing-Mechanism

Evaluation of performance of the previous piston designs indicated one fault common to all previous piston designs might exist without detection. It was the movement of the front polyethylene piston (Figure 4-1) during the period of disconnecting from the rear assembly through the recessing of the collapsing mechanism. Should the front piston exhaust its energy during this period, it might reverse its course causing a sudden drop in chamber pressure. Thus, a variable recessing-rate collapsing-mechanism capable of retarding the push of the rear piston assembly, but continuously exerting a mild pressure on the front piston during the period of retardation, was highly desirable.

Several mechanisms were proposed and statically tested. A simple Lexan cylinder drilled with a given number of holes along its longitudinal axis fitted the requirement. For example, a 2-in. dia cylinder of .5-in thick material drilled with 24 evenly spaced 0.312-in. holes along its longitudinal axis, started to displace under static axial load equivalent to 5,000 psi at the ends. The test specimen was contained in a heavy-walled steel pipe while

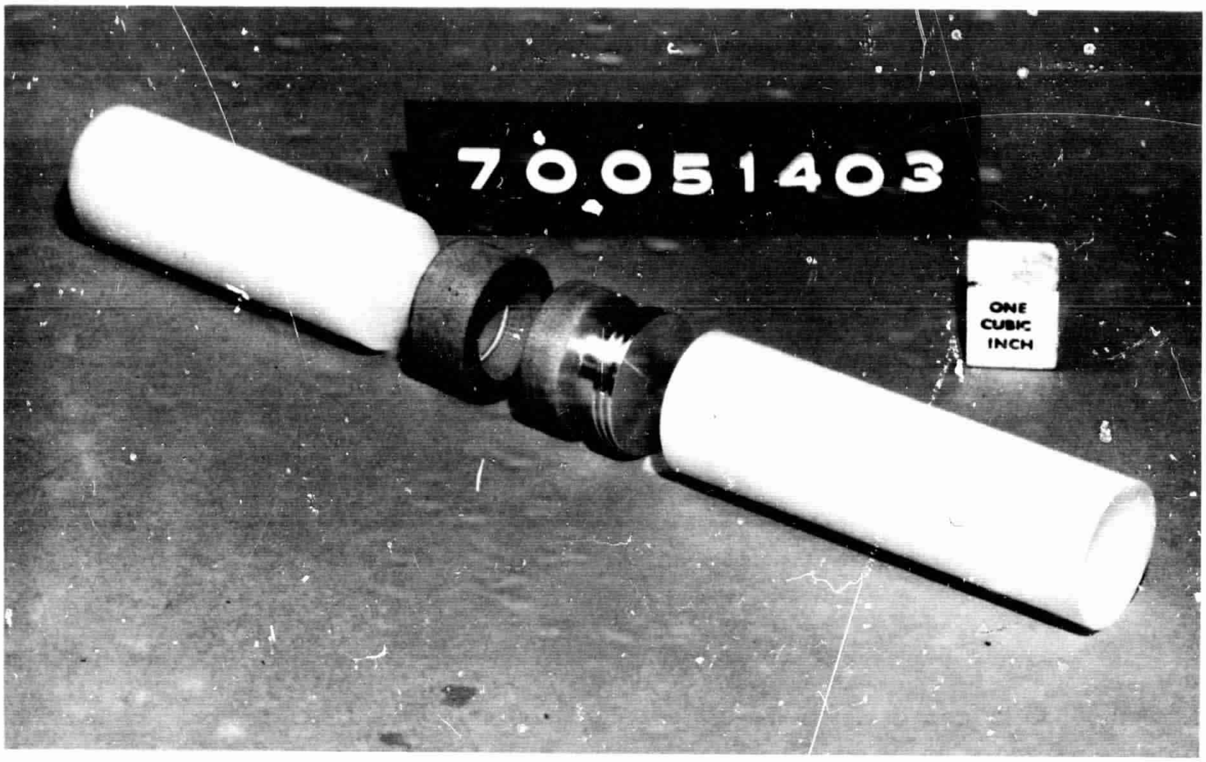

Figure 4-5. Glass-Reinforced Epoxy Collapsing-Mechanism

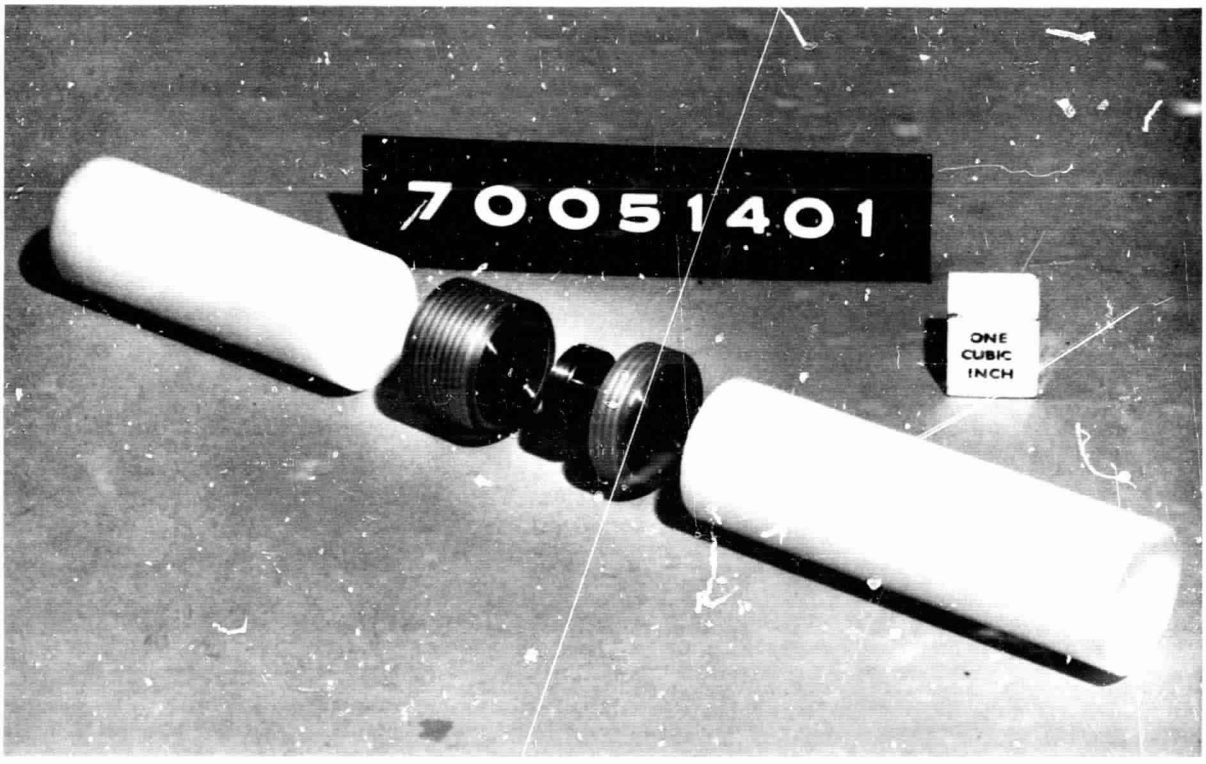

Figure 4-6. 17-4PH Stainless Steel Collapsing Mechanism

subjected to this load. The displacement did not stop until the load rose to a pressure of 30,000 psi on the ends.

Twelve shots have been run to verify the variable-recessing rate collapsing-mechanisms. The results have been very promising. Figure 4-7 shows a typical piston of this type. The center piece had been subjected to a static load equivalent of 20,000 psi on its ends.

4.5 MISCELLANEOUS RUNS

Many runs were made during the piston design evaluations to establish base lines and to remove uncertainties such as effects of leaks, component deformation, and instrumentation failures.

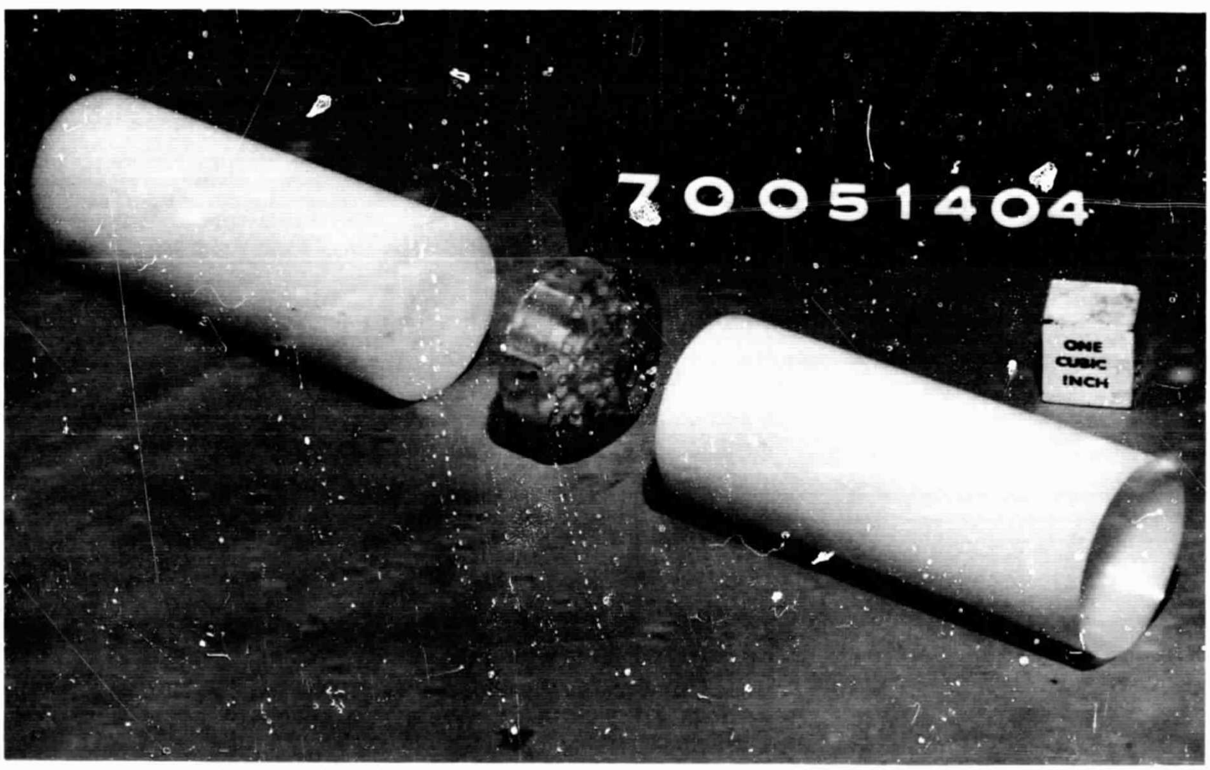

Figure 4-7. Variable Recessing-Rate Collapsing-Mechanism

Section 5
CONCLUSIONS AND RECOMMENDATIONS

The concept of approximating the constant base-pressure launch-cycle in a light-gas gun has been demonstrated to be feasible both theoretically and experimentally. However, during the early portion of the program some significant discrepancies between the theory and the experiment were found. Physical evidences such as the phenomena of the piston rebounding into the pump tube during some of the runs, the difficulties encountered in piston removal after the runs, and the appearance of the piston assembly after being freed from the pump tube all indicated the dominance of friction, which, in the theory of the constant base-pressure launch-cycle, was assumed to be small. A rough calculation using the shear stress value of the piston material to approximate the friction between the wall of the chamber and the piston assembly confirmed the conclusion derived from the physical evidences. The modified piston designs (Figures 4-3 through 4-7), employing the principle of molting, successfully overcame the problem of friction and yielded much higher muzzle velocities.

Unfortunately, there is no simple mathematical model for friction that can be included in the analysis of the launch cycles. But, it is believed that there exists a piston whose kinetic energy (correct mass and and velocity combination), together with the collapsing mechanism, is optimum to produce a near constant base-pressure launch-cycle. This optimum piston velocity is always higher than the theoretical value because of the friction. The smaller the piston friction the closer the constant base-pressure launch-cycle can be approached.

The collapsible-piston mechanism functioned as expected. For a given loading condition, the muzzle velocity increases as the collapsing distance decreases. Zero collapsing distance corresponds to a solid piston. It was concluded that for an identical life span of the gun components, launch cycles incorporating the collapsible piston assemblies yielded higher muzzle velocities than the solid pistons. Also, the maximum muzzle velocity achievable by a given gun can be extended by incorporating a collapsible piston of proper design.

In the routine operation of an ordinary two-stage light-gas gun, the piston is often ballasted by weights to achieve proper mass. The weight housings usually contain voids which in some ways function similarly to the variable-recessing rate collapsing-mechanism to effectively damp out the sharp pressure peaks.

The very high rupture pressure of the launch-tube diaphragm (over 30,000 psi) has an important effect on the gun performance (Figure 4-2). Higher diaphragm burst pressure yields higher muzzle velocity. However, ordinary projectile materials such as Lexan and polyethylene cannot survive extremely high shock-loading conditions. It is recommended that an experimental investigation of stronger projectile materials such as magnesium lithium be conducted. Since friction of the piston has been identified as the main obstacle to the successful operation of the constant base-pressure light-gas gun, it is recommended that an experimental program be initiated to develop a piston with either negligible or predicatable friction.

The sound speed of the hydrogen, an important factor in gun performance, may be significantly in error with the ideal gas assumption. Hence, it is further recommended that a real gas model, coupled with the collapsible piston concept, be incorporated into the analysis of the constant base-pressure launch-cycle. This improved theory should yield higher muzzle velocities and lower peak pressures in the gun than those simplified analyses employing either an ideal gas with collapsible piston or a real gas with solid piston.

Section 6

REFERENCES

1. J. S. Curtis. An analysis of the Interior Ballistics of the Constant Base Pressure Gun. Proceedings, Third Hypervelocity Techniques Symposium, Denver Research Institute, University of Denver, Denver, Colorado, March 1964, pp 423.

2. G. Witenius, M. Cloutier, and P. L. Cowan. A Theoretical Analysis of a Constant Base Pressure Light Gas Gun. Canadian Armament Research and Development Establishment, TM 703/62, Valcartier, Quebec. October 1962.

3. J. Lukasiewicz. Constant Acceleration Flows and Applications to High Speed Guns. AIAA Journal 5 No. 11 p 1955.